

Flavoured jets with exact anti- k_t kinematics and tests of infrared and collinear safety

Fabrizio Caola,¹ Radosław Grabarczyk,¹ Maxwell L. Hutt,^{1,2} Gavin P. Salam,^{1,3} Ludovic Scyboz,¹ and Jesse Thaler⁴

¹*Rudolf Peierls Centre for Theoretical Physics, Parks Road, Oxford OX1 3PU, UK*

²*The Blackett Laboratory, Imperial College London, Prince Consort Road, London, SW7 2AZ, UK*

³*All Souls College, Oxford OX1 4AL, UK*

⁴*Center for Theoretical Physics, Massachusetts Institute of Technology, Cambridge, MA 02139, USA*

We propose extensions of the anti- k_t and Cambridge/Aachen hierarchical jet clustering algorithms that are designed to retain the exact jet kinematics of these algorithms, while providing an infrared-and-collinear-safe definition of jet flavour at any fixed order in perturbation theory. Central to our approach is a new technique called Interleaved Flavour Neutralisation (IFN), whereby the treatment of flavour is integrated with, but distinct from, the kinematic clustering. IFN allows flavour information to be meaningfully accessed at each stage of the clustering sequence, which enables a consistent assignment of flavour both to individual jets and to their substructure. We validate the IFN approach using a dedicated framework for fixed-order tests of infrared and collinear safety, which also reveals unanticipated issues in earlier approaches to flavoured jet clustering. We briefly explore the phenomenological impact of IFN with anti- k_t jets for benchmark tasks at the Large Hadron Collider.

CONTENTS

I. Introduction	1	2. Recursive v. non-recursive	25
II. Reminders about existing jet algorithms	2	C. IRC-unsafe configurations	25
A. Flavourless kinematic clustering	2	1. IHC×IDS subtlety at α_s^3 for flavour- k_t	25
B. Flavour via recombination scheme	3	2. IHC ² issue at α_s^2 for CMP	27
C. Existing flavoured jet algorithms	4	3. IHC×IDS issue at α_s^3 for CMP	29
1. Flavour- k_t	4	4. FHC ² issue at α_s^2 for GHS	29
2. Flavour anti- k_t (“CMP”)	4	5. IDS×FDS issue at α_s^4 for GHS	31
3. Flavour dressing (“GHS”)	4	D. Summary plots for IRC-safe algorithms	32
4. Multi-flavoured events	5	References	35
III. Anti- k_t and C/A jets with interleaved flavour neutralisation	5		
A. Design aims and core concept	5		
B. Introducing the IFN algorithm	6		
C. Choice of neutralisation distance	7		
D. Need for recursion	9		
E. Further comments	9		
IV. IRC safety: discussion and tests	9		
A. Methodology	10		
B. Classes of IRC emissions	10		
C. Implementation details	12		
D. Results	13		
V. Phenomenological illustrations	16		
A. Heavy flavour in $pp \rightarrow WH(\rightarrow \mu\nu b\bar{b})$	17		
B. Heavy flavour in $pp \rightarrow t\bar{t} \rightarrow \ell\nu + \text{jets}$	18		
C. Full flavour at parton level in $pp \rightarrow Z + j$	19		
VI. Exploration of IFN algorithm for e^+e^- collisions	21		
VII. Conclusions and outlook	22		
Acknowledgements	23		
A. Asymmetric double-soft branching	23		
B. Numerical tests of IFN	24		
1. Relation between α and ω	24		

I. INTRODUCTION

The use of jet clustering algorithms is essential and ubiquitous at colliders. Jet algorithms relate collimated sprays of energetic hadrons to the underlying concept of hard, perturbative quarks and gluons (or, more generally, partons). In the vast majority of cases, only the kinematics of the resulting jets are used for analysis. Insofar as jets are meant to represent the underlying partonic structure of an event, though, it is natural to ask whether jets can also reflect the flavour of the underlying partons, for example their quark or gluon nature. The question of how to formulate a jet algorithm where the flavours assigned to jets are infrared and collinear (IRC) safe was first posed in 2006 [1, 2]. The algorithm developed there, flavour- k_t , based on a modification of the k_t algorithm [3–5], appeared to be successful in this task. However, one of the characteristics of flavour- k_t was that the kinematics of the resulting jets depended on the flavour of the underlying constituents being clustered.

In modern jet usage, where the subsequently developed anti- k_t algorithm [6] has found widespread applications, a flavour-induced modification of the jets’ kinematics is undesirable. Notably, it has been found to complicate

unfolding corrections [7]. Nevertheless, there are situations where IRC-safe flavoured jet algorithms would be highly beneficial. For example, the question of IRC-safe jet flavour has recently come to the fore in the context of heavy-flavour jets [8–11]. IRC safety in this instance ensures that flavoured jet cross sections do not contain any logarithms of the ratio of the jet transverse momentum p_t to the quark mass m_q . It also makes it possible to use an $m_q = 0$ approximation in fixed-order perturbative calculations [7, 12–21], with an expectation that any missing contributions are suppressed by powers of m_q/p_t .

In this article, we present a new strategy for flavoured jet finding called Interleaved Flavour Neutralisation (IFN), which is designed to combine an IRC-safe definition of jet flavour with the IRC-safe kinematics of sequential clustering. We will study IFN with two generalised- k_t -style jet algorithms, the anti- k_t algorithm, used extensively at the Large Hadron Collider (LHC), and the Cambridge/Aachen (C/A) algorithm [22, 23], widely favoured for jet substructure studies. In the case of the anti- k_t algorithm, our objectives are similar to those of the recent “flavoured anti- k_t ” [10] and “flavour dressing” [11] algorithms, which respectively achieve approximate and exact anti- k_t (or C/A) kinematics, but because it integrates flavour information at each stage of the clustering sequence, it is a viable candidate for jet substructure studies. We also carry out a much more extensive set of IRC safety tests than in any prior work, which support the conclusion that IFN is IRC safe, at least through order α_s^6 . These tests also reveal unexpected and subtle issues in the default formulations of all prior flavoured jet algorithms.

We focus on the theoretical definition of jet flavour, leaving a study of experimental issues to future work. The extent to which any IRC-safe flavour algorithm can be adopted experimentally is an open question. Even when identifying heavy-flavour jets, where collinear singularities are regulated by a non-zero m_q , such algorithms would typically require the identification of all heavy-flavoured hadrons in an event. That is challenging when there are multiple heavy-flavoured hadrons in a single jet, or when some of the heavy-flavoured hadrons have low momenta.¹ Despite these experimental subtleties, the underlying question of IRC-safe flavour identification remains conceptually important. Jet flavour can provide a valuable tool in a range of theoretical work, for example in matching parton showers and fixed-order calculations [24]. One can further anticipate that it will be useful in testing logarithmic accuracy for flavour-related aspects of parton showers [25, 26].

The remainder of this article is organised as follows. In Sec. II, we review the key features of widely-adopted jet algorithms, and some of the issues that arise when

flavour tagging is sought. We also briefly describe existing proposals for those flavoured jet algorithms that aim to achieve all-order IRC safety [1, 2, 10, 11]. In Sec. III, we outline our general design aims for a modern flavoured jet algorithm and present a concrete realisation via IFN. That section also includes a discussion of some of the subtle considerations brought about by IRC-safety requirements. In Sec. IV, we present the framework that we developed to explore IRC-safety issues in some depth (a substantial extension of the approach developed some time ago for testing the SIScone jet algorithm [27]), which we apply both to our IFN proposal and to earlier flavoured jet algorithms. These tests expose unanticipated issues in earlier proposals, many of them connected with the treatment of initial-state radiation in a hadron collider context. In some cases, we identify simple adaptations of the original algorithms that should make them IRC safe. In Sec. V, we perform three benchmark phenomenological studies to illustrate the behaviour of various flavoured jet algorithms, restricting ourselves to the ones that pass our IRC-safety tests. In Sec. VI, we briefly present the adaptation of our approach to e^+e^- colliders. We conclude in Sec. VII.

Additional material is presented in the appendices. In App. A, we review some features of the double-soft quark emission current that we used for our analyses. In App. B we perform numerical tests to justify some of the design decisions we made for the IFN algorithm. In App. C, we provide detailed analyses of the main IRC-safety issues that we encountered in this work. In App. D, we present summary plots of IRC-safety tests for those algorithms that we expect to be IRC safe.

II. REMINDERS ABOUT EXISTING JET ALGORITHMS

In this section, we briefly review standard jet algorithms and their interplay with jet flavour, including the original flavour- k_t approach [1]. To avoid confusion, we refer to the flavoured anti- k_t algorithm of Ref. [10] as “CMP”, and the flavour dressing algorithm of Ref. [11] as “GHS”. Throughout this section and most of this article, we concentrate on longitudinally invariant hadron-collider algorithms, with a brief mention of an e^+e^- adaptation in Sec. VI.

A. Flavourless kinematic clustering

Let us start with a reminder of how the generalised- k_t algorithm works. It employs distances d_{ij} between each pair of pseudojets² i and j and d_{iB} between each

¹ Though as we will see in Sec. VB for the $t\bar{t}$ process, this may be less of an issue than one might fear.

² Recall that a pseudojet may be either a single particle or the combination of more than one particle arising from an earlier stage of the clustering.

pseudojet i and the beam:

$$d_{ij} = \min(p_{ti}^{2p}, p_{tj}^{2p}) \frac{\Delta R_{ij}^2}{R^2}, \quad (1a)$$

$$\Delta R_{ij}^2 = (y_i - y_j)^2 + (\phi_i - \phi_j)^2, \quad (1b)$$

$$d_{iB} = p_{ti}^{2p}, \quad (1c)$$

where p_{ti} , y_i and ϕ_i are respectively the transverse momentum, rapidity and azimuth of i ($y_i = \frac{1}{2} \ln \frac{E_i + p_{zi}}{E_i - p_{zi}}$). The algorithm has two parameters, the jet radius R , which sets the angular reach of the jets, and the power p , which sets the nature of the algorithm: -1 , 0 , 1 respectively for the anti- k_t [6], Cambridge/Aachen [22, 23] and k_t algorithms [4, 5]. The algorithm starts with all event particles and proceeds as follows:

1. identify the smallest of the d_{ij} and d_{iB} among all i and j at this stage of the clustering;
2. if it is a d_{ij} , recombine i and j into a single new pseudojet and return to step 1;
3. if it is a d_{iB} , declare i to be a jet and remove it from the list of pseudojets to be considered at subsequent clustering steps; return to step 1.

The clustering stops once no pseudojets are left to be clustered. Given the resulting jets, it is common to consider only the subset that pass minimum p_t (and maximum rapidity or pseudo-rapidity³) constraints.

B. Flavour via recombination scheme

A crucial element of the jet definition is the choice of recombination scheme. The most common is the (somewhat inappropriately named) E scheme, in which 4-momenta are simply added. Flavour is usually not considered within standard jet algorithms, but it is useful to introduce three potential flavour recombination schemes:

- **Any-flavour scheme:** This scheme is relatively close to typical experimental practice for b - and c -tagging. Here, any recombination that involves non-zero flavour, e.g. $q + g$, $\bar{q} + g$, or $q + \bar{q}$, yields a flavoured result. From a theoretical point of view, this scheme is collinear unsafe for massless quarks due to the collinear divergence of $g \rightarrow q\bar{q}$ splitting. For massive quarks, as in the case of b and c production, this scheme is logarithmically sensitive to the quark mass. We will further consider this “any-flavour” scheme only in a phenomenological context in Sec. VB.

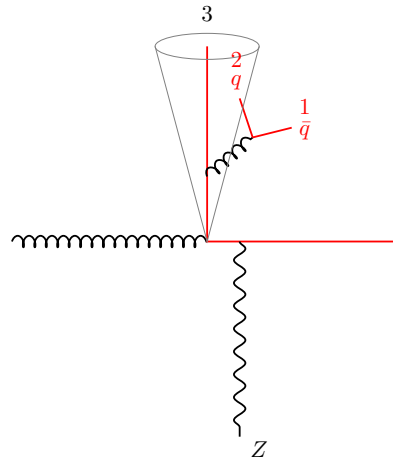


FIG. 1. Classic problematic flavour configuration at NNLO. A soft gluon at large angle splits to a $q\bar{q}$ pair (labelled 1 and 2), and the flavour of the hard jet (numbered 3) is polluted by the flavour of 2, while 1 ends up outside the jet.

- **Net-flavour scheme:** This is a theoretically better-motivated scheme that considers the net flavour in the recombination. In this scheme, a q carries flavour, a \bar{q} carries anti-flavour, and a $q\bar{q}$ carries no flavour. This “net-flavour” scheme resolves the collinear unsafety for $g \rightarrow q\bar{q}$ splitting.
- **Flavour modulo-2 scheme:** Typically for heavy flavour at hadron level, it is not conceptually possible to distinguish flavour from anti-flavour, e.g. because of $B_0 - \bar{B}_0$ oscillations. In such a situation, one may consider a “flavour modulo-2” scheme (see e.g. Ref. [2]). Specifically, b and \bar{b} are treated as equivalent while $b\bar{b}$, $b\bar{b}$ and $\bar{b}\bar{b}$ are all considered to be flavourless. This scheme also resolves the issue of collinear unsafety for $g \rightarrow q\bar{q}$ splitting.

While the net flavour and modulo-2 options ensure that the jet flavour is unaffected by collinear divergences for $g \rightarrow q\bar{q}$ splittings, they still exhibit IRC safety issues for jet flavour at higher orders, at least when used with standard jet algorithms. This occurs at next-to-next-to-leading order (NNLO), as discussed in Ref. [1] and illustrated in Fig. 1 (see App. A for further discussion about the matrix element for this process). Specifically, when a soft gluon splits to a large-angle $q\bar{q}$ pair, one or other of the resulting soft quarks can be clustered with a hard jet and the net-flavour and modulo-2 recombination schemes result in an IRC-unsafe flavour for hard jets, with the divergence appearing as $\alpha_s^2 \ln p_{t,\text{jet}}/m_q$ for a finite quark mass m_q . This is the classic problem when attempting to obtain IRC-safe jet flavour.

When considering more than one flavour (e.g. all of u, d, s, c, b), flavour recombination is typically applied separately for each flavour. This may be done either within a single run of the algorithm or (for algorithms where the flavour does not affect the jet kinematics) applying the

³ The jets may be massive, and as a result pseudo-rapidity is not advised [28].

flavour part of the jet clustering in one separate run of the algorithm for each kind of flavour.

C. Existing flavoured jet algorithms

We now review three jet-flavour definitions that aim to achieve all-order IRC safety (see Refs. [8, 9, 29] for alternative definitions of jet flavour).

1. Flavour- k_t

The flavour- k_t [1] algorithm took the approach of using a net or modulo-2 flavour scheme, while modifying the clustering distances relative to Eq. (1). Specifically, it modifies the standard k_t ($p = 1$) distance when the softer of i and j is flavoured

$$d_{ij}^{\text{flav-}k_t} = [\max(p_{ti}, p_{tj})]^\alpha [\min(p_{ti}, p_{tj})]^{2-\alpha} \frac{\Delta R_{ij}^2}{R^2}, \quad (2)$$

if softer of i and j is flavoured,

with the parameter α usually taken to be 1 or 2.⁴ This has the consequence that the d_{ij} for the clustering of a soft flavoured particle with a significantly harder particle is much larger than the d_{ij} for two similarly soft particles. As a result, the soft particles cluster first, resolving the original IRC safety issue of Fig. 1. Note that flavour- k_t also uses a modified d_{iB} distance for flavoured particles. The details are best obtained from the original article [1], however the essence of the modified beam distance is that one uses the same kind of construction as in Eq. (2),

$$d_{iB}^{\text{flav-}k_t} = [\max(p_{ti}, p_{tB}(y_i))]^\alpha [\min(p_{ti}, p_{tB}(y_i))]^{2-\alpha}, \quad (3)$$

with $p_{tB}(y)$ a rapidity-dependent hardness scale. In the central region, $p_{tB}(y)$ is of the same order as the overall event hardness.

Relative to the standard k_t algorithm, the flavour- k_t algorithm can significantly alter the kinematics of the clustering of hard flavoured jets. For example in the presence of a hard $b\bar{b}$ pair, the flavour- k_t algorithm can cluster them even when $\Delta R_{b\bar{b}} > R$, as observed e.g. in Ref. [32] (see also the discussion in Sec. V A).

2. Flavour anti- k_t (“CMP”)

The algorithm of Ref. [10], there called “flavour anti- k_t ”, will be referred to here as CMP, to avoid ambiguity

with other flavour anti- k_t algorithms. As in the flavour- k_t algorithm, it is to be used with net-flavour or modulo-2 flavour recombination. It modifies the anti- k_t ($p = -1$) d_{ij} distance when i and j are oppositely flavoured

$$d_{ij}^{\text{flav-anti-}k_t} = d_{ij}^{\text{anti-}k_t} \times \mathcal{S}_{ij}, \quad (4)$$

if i and j are oppositely flavoured,

where

$$\mathcal{S}_{ij} = 1 - \Theta(1 - \kappa) \cos\left(\frac{\pi}{2}\kappa\right), \quad \kappa \equiv \frac{1}{a} \frac{p_{ti}^2 + p_{tj}^2}{2p_{t,\max}^2}, \quad (5)$$

and $p_{t,\max}$ would typically be a hard scale (see Ref. [10] for further details). Throughout this paper, we use $p_{t,\max} \equiv p_{t,\text{global-max}}$, where $p_{t,\text{global-max}}$ is the transverse momentum of the hardest pseudojet across the event at the given stage of the clustering.⁵ In addition to the jet radius, the algorithm has one parameter, a , taken in the range 0.01–0.5 in the original publication [10]. Unlike the flavour- k_t algorithm, the CMP algorithm uses a beam distance that is identical to that of the plain anti- k_t algorithm.

The CMP algorithm resolves the problem in Fig. 1 because when particles 1 and 2 are both soft, κ is very small. Specifically, taking dimensions such that $p_{t,\text{global-max}} = 1$, a soft ij quark pair has $\mathcal{S}_{ij} \sim \kappa^2 \sim \max(p_{ti}^4, p_{tj}^4)$, leading to an overall $d_{ij} \sim \max(p_{ti}^2, p_{tj}^2) \Delta R_{ij}^2$. This is much smaller than the anti- k_t clustering distance of a soft quark with a hard parton, which is of order ΔR_{ij}^2 . As a result the soft $q\bar{q}$ pair clusters first and there is no IRC-safety issue in Fig. 1. Note that when one or other of i and j is hard, the use of a small value for the parameter a results in κ being large and thus $\mathcal{S}_{ij} = 1$. As a result, the CMP algorithm behaves like the anti- k_t algorithm for hard particles. For $a \rightarrow 0$, the algorithm reduces to anti- k_t . However, for finite a , the algorithm does sometimes yield jets whose kinematics differ from those of the anti- k_t algorithm.

3. Flavour dressing (“GHS”)

The algorithm of Ref. [11], there called “flavour dressing”, will be referred to here as GHS. This algorithm involves three stages: a standard clustering stage in which flavour is not considered, an “accumulation” stage in which flavoured particles accumulate momentum from non-flavoured ones, and a “dressing” stage, which assigns the flavour to the original anti- k_t jets. Here, we limit ourselves to sketching the main features of each of the steps, and refer the reader to the original reference for the full details.

⁴ The $\alpha = 1$ variant evokes a longitudinally-invariant extension of the classic JADE (squared invariant mass) clustering distance [30, 31]. The well-known drawback of the JADE distance, namely that early in the sequence it can cluster soft pairs going in opposite directions, is precisely the behaviour needed to resolve the classic jet-flavour IRC safety issue of Fig. 1.

⁵ We are grateful to the authors of Ref. [10] for discussions on this point.

In the first step, the event is clustered with the standard anti- k_t algorithm. In this step, one also applies standard jet cuts, e.g. on transverse momentum and rapidity, to the resulting jets.

In the second step, the algorithm runs an “accumulation” stage, which follows a version of C/A clustering (i.e. $p = 0$ in Eq. (1a)) with a radius of R_{cut} , with two modifications: (i) clustering of flavoured objects with non-flavoured ones discards the non-flavoured one if the clustering fails to pass a SoftDrop kinematic cut [33],

$$\frac{\min(p_{ti}, p_{tj})}{(p_{ti} + p_{tj})} > z_{\text{cut}} \left(\frac{\Delta R_{ij}}{R_{\text{cut}}} \right)^\beta, \quad (6)$$

where z_{cut} and β are the usual SoftDrop parameters; (ii) when two flavoured objects would normally cluster, they are instead both removed from the accumulation clustering process and each is treated as a “flavour cluster”, to be used as an input to the third step of the algorithm. Any flavoured clusters that remain at the end of the modified C/A clustering also serve as inputs to the third step.

The third step is the flavour “dressing” itself. It evaluates flavour- k_t distances (a) between pairs of flavour clusters ($d_{\hat{f}_i \hat{f}_j}$), (b) between each flavour cluster and the anti- k_t jet, j_k , to which the flavoured particle in the cluster belonged ($d_{\hat{f}_i j_k}$) and (c) with the beam ($d_{\hat{f}_i B\pm}$). When the smallest distance is a $d_{\hat{f}_i \hat{f}_j}$, the flavours annihilate and \hat{f}_i and \hat{f}_j are removed from further consideration; when it is a $d_{\hat{f}_i j_k}$, the flavour of i is assigned to jet j_k and \hat{f}_i is removed from further consideration; and when it is a $d_{\hat{f}_i B\pm}$, \hat{f}_i is simply discarded. Distance measures involving any flavour clusters \hat{f}_i or \hat{f}_j that were annihilated, assigned or discarded are then removed from the list, and the procedure repeats until no flavoured clusters remain. Besides the standard jet radius, the algorithm has four parameters: R_{cut} , associated with the C/A clustering, β and z_{cut} for the SoftDrop condition, and the α of the flavour- k_t distances.

In the configuration of Fig. 1, we would have three flavour clusters (1, 2, 3), with 2 and 3 associated with a hard jet. The third step of the algorithm would annihilate the \bar{q} and q flavours of 1 and 2, because they have the smallest flavour- k_t distance, and attribute the flavour of 3 to the hard jet. The flavour dressing algorithm never modifies the kinematics of the original anti- k_t jets, only their flavour. Note that for events where every anti- k_t jet consists of a single particle, i.e. events where there has been no kinematic recombination, the flavour of each jet is the same as for the anti- k_t algorithm. This is a property that we will seek also in our IFN algorithm.

4. Multi-flavoured events

A final comment concerns clustering of events with more than one flavour (e.g. tracking both b and c flavour). The flavour- k_t algorithm is to be run with all flavours for

which one wants information in the final jets. The CMP and GHS algorithms are designed for a single flavour at a time (e.g. just the b and \bar{b} flavour in the event). However, we note that for the CMP algorithm it is straightforward to identify potential ways of extending it, for example by using the distance in Eq. (4) whenever a pair has the potential for at least some cancellation of flavour. As concerns GHS, since it does not modify the anti- k_t jets’ kinematics, one can simply re-run it again for a second flavour, and so forth.

III. ANTI- k_t AND C/A JETS WITH INTERLEAVED FLAVOUR NEUTRALISATION

In this section, we present the motivation for, and description of, our new flavour neutralisation algorithm.

A. Design aims and core concept

If we consider what is needed for broad usage of a jet flavour algorithm, we can identify at least four criteria that are necessary, or at least highly desirable:

1. **IRC safety:** Both the kinematics and the flavours of any hard jets should be IRC safe.
2. **Preserved kinematics:** For a given member of the generalised- k_t algorithm family, the flavour algorithm should not modify the jets’ kinematics.
3. **Multi-scale flavour resolution:** The flavours of the pseudojets should be well defined at any step of the clustering, so as to leave open the possibility of using flavour information with the full cluster sequence, e.g. for jet substructure studies.

Additionally, as mentioned at the end of Sec. II C 3, it can be beneficial to have the following property:

4. **Single parton consistency:** For events in which each jet contains exactly one parton, the flavour algorithm should not modify the jets’ flavours relative to the simple generalised- k_t algorithm. This ensures that typical leading-order calculations will give the same results for the generalised- k_t algorithm and its flavoured extension. It notably means that one cannot a priori decide to neglect some subset of flavour in an event without specifying the jet kinematics.

To achieve these aims, the core novel idea that we introduce here is that of maintaining the standard clustering procedure, but modifying the flavour-related aspects of the recombination scheme at each step of kinematic recombination. In particular, our approach uses a global, event-wide treatment of flavour at each pair-wise clustering step. By construction, the resulting jets will have identical kinematics as compared to the original jet algorithm, and we aim to arrange for the flavour labels

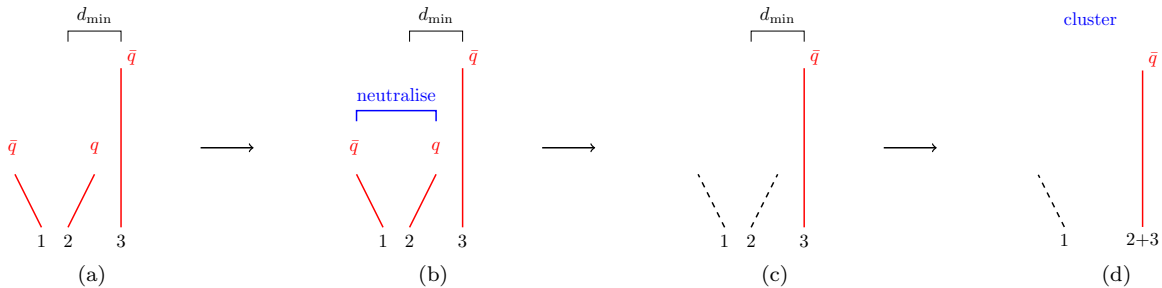


FIG. 2. Illustration of the flavour-neutralisation approach. The event displayed here (a) has the property that there is a soft $\bar{q}q$ pair (particles 1 and 2), and a hard \bar{q} (particle 3) with $p_{t1} \sim p_{t2} \ll p_{t3}$. Additionally, we have all ΔR distances of order one, but with the constraint that $\Delta R_{23} < R$, while $\Delta R_{12} > R$, so that within the anti- k_t algorithm, 2 and 3 cluster into one jet, while 1 would form a separate soft jet. In (b), just before the $2+3$ clustering, the flavour of 1 is used to neutralise the flavour of 2, which results in the intermediate stage shown in (c), where particles 1 and 2 have lost their flavour (as represented by the black dashed lines). Finally, in (d) the (now) flavourless pseudojet 2 is clustered with 3 into a pseudojet $2+3$ with the \bar{q} flavour of just particle 3.

associated with the jets to be IRC safe at any stage in the clustering sequence.

There is quite some freedom in such an approach. The fundamental principle of flavour neutralisation, which we believe can be applied in a variety of ways, is illustrated in Fig. 2. When a pseudojet with non-zero flavour is about to undergo a kinematic clustering (soft q (2), clustering with hard \bar{q} (3) in Fig. 2a), the algorithm needs to establish whether the flavours of 2 and 3 should be combined as per usual net-flavour summation, or instead whether the flavour of either of the particles should be “neutralised” by some other particle(s) in the event before allowing the kinematic $(2+3)$ clustering to proceed. For example, in Fig. 2b, with a soft \bar{q} (particle 1) in the vicinity of the soft q (2), the algorithm may decide to first neutralise the flavours of particles 1 and 2, before moving ahead with the $2+3$ clustering. If that neutralisation happens, then particles 1 and 2 become flavourless, as illustrated by the black dashed lines in Fig. 2c. This is then followed by the kinematic clustering in Fig. 2d, resulting in a $2+3$ jet that retains the \bar{q} flavour of hard particle 3, as needed for IRC safety.

In general, the IRC safety (or otherwise) of the algorithm resides in the criteria used to decide whether to neutralise a given pseudojet’s flavour, and if so then with which other pseudojet(s). As with earlier flavoured clustering algorithms, such a procedure will need to rely on some measure of the likelihood that a given flavoured pair came from an effective parent gluon’s splitting, versus the flavour originating from a genuine hard parton.

B. Introducing the IFN algorithm

We now construct a concrete algorithm based on Fig. 2 that integrates jet clustering with flavour neutralisation: Interleaved Flavour Neutralisation (IFN). The core of our algorithm is the search for neutralisation candidates at

any given stage of the clustering. Among the ingredients of that search is a measure of flavour neutralisation distance u_{ij} between any pair of particles i and j , the softer of which will always be flavoured. For now, the reader may wish to think of u_{ij} as being a flavour- k_t type distance, cf. Eq. (2), though there are important further subtleties, discussed below in Sec. III C.

In defining the algorithm in the next few paragraphs, we shall frequently make reference to Fig. 2 to illustrate the function of the different steps, keeping in mind that the flavour of the final hard jet (made of particles 2 and 3) should ultimately just be that of the hard particle $3_{\bar{q}}$ without contamination from the flavours of the soft $1_{\bar{q}}2_q$ pair.

We write the core neutralisation search part of the algorithm in the style of a computer subroutine $N(i, u_{\max}, C, E)$, taking a number of arguments as inputs, specifically:

- the index i of the pseudojet for which to identify potential neutralisation partner(s) (e.g. $i = 2$ in Fig. 2a);
- a threshold u_{\max} above which to ignore neutralisation candidates (e.g. in the context of the $2+3$ kinematic clustering in Fig. 2a this would be $u_{\max} = u_{23}$);
- a list C of all potential neutralisation candidates, i.e. all currently flavoured pseudojets in the event ($C = \{1, 2, 3\}$ in Fig. 2a);
- a subset E among those flavoured pseudojets to be excluded in the neutralisation search because they have already been considered in some prior step of the algorithm ($E = \{2, 3\}$ in Fig. 2a, because particles 2 and 3 have already been considered in that they set $u_{\max} = u_{23}$).

The $N(i, u_{\max}, C, E)$ algorithm is formulated as follows:

- N1. Create a list L of u_{ik} distances for all k among the candidates C that satisfy $u_{ik} < u_{\max}$, excluding those in the exclusion set E .
- N2. Identify the k that corresponds to the smallest u_{ik} in the list.
- N3. If k contains no flavour that can neutralise flavour in i (e.g. k is a b -quark and i is a c -quark), remove the corresponding u_{ik} from list L , and loop back to step N2.
- N4. Before using k to neutralise flavour in i , check to see whether there are other pseudojets that could more naturally be paired with k in order to neutralise k 's flavour. Do so through a recursive use of flavour neutralisation, searching for neutralisation partners of k by running $N(k, u_{ik}, C, E \cup \{k\})$. Sec. III D explains the importance of recursion for IRC safety.
- N5. For each flavour currently in i , neutralise as much of that flavour as one can with any flavour that is still present in k .⁶ For example, if i has flavour $c\bar{b}$ and k has flavour $b\bar{b}$, use k to cancel the \bar{b} flavour, so that the updated i has flavour c and the updated k has flavour b .
- N6. If i is now flavourless, exit.
- N7. Otherwise remove the current u_{ik} from list L . If any entries are still left in list L , loop back to step N2. Otherwise exit.

In our IFN formulation, the flavour neutralisation search is triggered whenever a clustering is about to occur for which the softer pseudojet is flavoured, specifically:

- I1. When pseudojets i and j recombine in the standard kinematic clustering sequence, let i be the pseudojet with lower p_t . If i is flavourless, then $i+j$ simply takes the flavour of j and one moves on to the next kinematic jet clustering step.
- I2. Otherwise, identify all pseudojets that currently carry flavour, including any flavoured jets declared earlier according to a d_{iB} step, and put them into a list C of potential neutralisation candidates. Initialise the set $E = \{i, j\}$ of particles to be excluded from the search for neutralisation candidates.
- I3. Call the flavour-neutralisation search, $N(i, u_{ij}, C, E)$, which may use one or more flavoured particles in set C to neutralise some or all of the flavour contained in i .

- I4. For any remaining flavour in i , apply the standard net-flavour (or flavour modulo-2) summation of i with j and move on to the next kinematic jet clustering step.

Interleaving flavour neutralisation at each step of the clustering is important from the point of view of collinear safety. To illustrate this, it is helpful to suppose that particles i , j and k all have comparable transverse momenta and inter-particle distances $\Delta R \sim R$. In this situation $u_{ij} \sim u_{ik}$. Consider the case where j undergoes a collinear splitting, $j \rightarrow j_a, j_b$ with $\Delta R_{j_a, j_b} \ll R$. If one ran flavour neutralisation without clustering, one could find oneself in a situation where $u_{ik} < u_{ij}$, but $u_{ik} > u_{ij_a}$, thus changing the neutralisation sequence.

Now let us examine how this changes if neutralisation is interleaved with clustering. The clustering algorithms that we consider are the anti- k_t and C/A algorithms. They both have the property that when all particles have similar transverse momenta, clustering of the collinear j_a, j_b pair will precede the ij clustering step. At the j_a, j_b clustering, if the neutralisation search gets triggered, then j_a and j_b will cluster with normal net-flavour recombination, since $u_{j_a j_b}$ is much smaller than all other u 's. When the clustering reaches the ij step, all distances will see the kinematics of j , rather than that of the underlying j_a and j_b , thus ensuring that the algorithm is collinear safe.⁷

C. Choice of neutralisation distance

Let us now turn to the u_{ik} flavour neutralisation distance between a pair of particles i and k . Recall that the softer of the two will always be flavoured, while the harder one may or may not be.

We write the u_{ik} distance generically with two parameters, α and ω :

$$u_{ik} \equiv [\max(p_{ti}, p_{tk})]^\alpha [\min(p_{ti}, p_{tk})]^{2-\alpha} \times \Omega_{ik}^2, \quad (7a)$$

$$\Omega_{ik}^2 \equiv 2 \left[\frac{1}{\omega^2} (\cosh(\omega \Delta y_{ik}) - 1) - (\cos \Delta \phi_{ik} - 1) \right], \quad (7b)$$

where $\Delta y_{ik} = y_i - y_k$ and analogously for $\Delta \phi_{ik}$. Let us start with the part related to the transverse momenta. This is identical to that used in the flavour- k_t algorithm, cf. Eq. (2), with the same parameter α . As in typical

⁶ If working with flavour modulo-2, then initial flavours are always to be understood as being modulo-2, and each comparison and/or combination is also to be performed in a modulo-2 sense.

⁷ When considering collinear splitting in events with a hierarchy of energies, the different members of the generalised- k_t family may perform the soft and the collinear clusterings in different orders. However, when the neutralisation search is, say, comparing neutralisation distances involving two soft particles i and k and a hard particle j ($u_{ik} \ll u_{ij}, u_{kj}$), a collinear splitting of any of the soft or hard particles will only modify the u 's by a factor of order 1 and it will leave the hierarchies untouched, and correspondingly also the resulting neutralisation pattern.

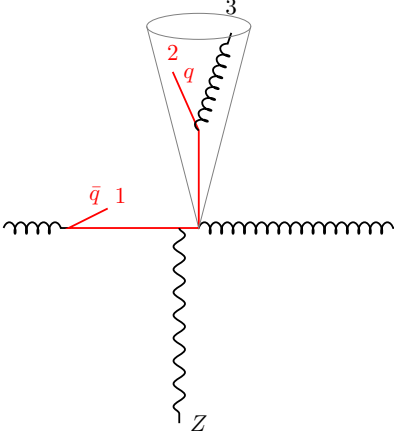


FIG. 3. NNLO contribution to the $pp \rightarrow Z + \text{jet}$ process, that helps illustrate the origin of the condition, Eq. (9), on the ω parameter in the angular part of the u_{ij} distance, Eq. (7a). It involves a hard jet with a final-state splitting (where the jet constituents, q and a gluon, are labelled 2 and 3 respectively), as well as an initial-state collinear splitting ($g \rightarrow q\bar{q}$, with the \bar{q} labelled 1). When $\alpha + \omega < 2$, the initial-state collinear \bar{q} (1) neutralises the flavour of the q (2).

flavour- k_t studies, we assume $0 < \alpha \leq 2$, and in particular concentrate on $\alpha = 1$ and $\alpha = 2$.

Next, we examine the angular part of the distance, Ω_{ik}^2 , which involves a parameter ω . For any ω of order 1, in the limit of small Δy_{ik} and small $\Delta\phi_{ik}$, Ω_{ik}^2 reduces to the standard $\Delta R_{ik}^2 = \Delta y_{ik}^2 + \Delta\phi_{ik}^2$. The reason for using Ω_{ik}^2 rather than the standard ΔR^2 is to ensure IRC safety as concerns the interplay between collinear initial-state splittings and splittings elsewhere in the event. This is best explained with the help of Fig. 3. In the anti- k_t and C/A algorithms, particles 2 and 3 will cluster first.⁸ When $p_{t2} < p_{t3}$, the 2 + 3 clustering triggers a flavour neutralisation search. The only candidate for flavour neutralisation is particle 1 and one should compare the u_{12} and u_{23} distances. We will suppose that particles 2 and 3 have similar p_t 's and are at central rapidity. The initial-state collinear splitting that creates particle 1 typically results in $y_1 = \ln p_{t3}/p_{t1} + \mathcal{O}(1)$. Neglecting $\mathcal{O}(1)$ factors, we then have

$$u_{12} \sim p_{t2}^\alpha p_{t1}^{2-\alpha} \left(\frac{p_{t3}}{p_{t1}} \right)^\omega \sim p_{t3}^{(\alpha+\omega)} p_{t1}^{(2-\alpha-\omega)}, \quad (8a)$$

$$u_{23} \sim p_{t3}^\alpha p_{t2}^{2-\alpha} \Delta R_{23}^2 \sim p_{t3}^2 \Delta R_{23}^2. \quad (8b)$$

where in the rightmost part of each equation we have exploited $p_{t2} \sim p_{t3}$. One immediately observes that if $\alpha + \omega < 2$, then in the initial-state collinear limit, where $p_{t1} \ll p_{t3}$, one has $u_{12} \ll u_{23}$. This causes particle 1

⁸ This would not be the case for the k_t algorithm, and an investigation of the interplay of k_t clustering with IFN is left to future work.

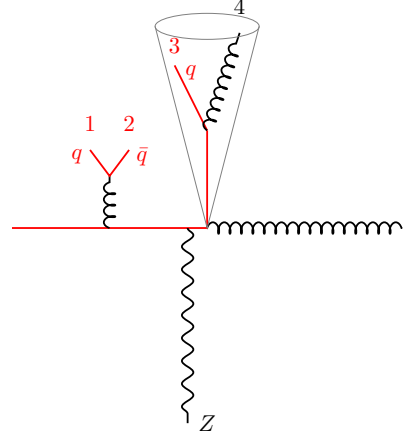


FIG. 4. N³LO contribution to the $Z + \text{jet}$ process that helps illustrate the need for recursion in step N4 of the flavour neutralisation search. It involves a hard jet with a non-collinear splitting (flavoured 3 and flavourless 4) and a flavoured initial-state double-soft pair (labelled 1 and 2). Without recursion, particle 2 can end up neutralising the flavour of 3.

to neutralise the flavour of particle 2, even when 1 is arbitrarily collinear, resulting in a flavourless hard jet. In contrast, when the initial-state splitting is absent, the hard jet will be flavoured. Thus, the algorithm would be unsafe with respect to initial-state collinear splittings. On the other hand, if we take

$$\alpha + \omega > 2, \quad (9)$$

then u_{12} will always be parametrically larger than u_{23} in the limit $p_{t1} \rightarrow 0$, thus effectively forbidding neutralisation of 1 and 2; see App. B 1 for further discussion.⁹ In practice, we will nearly always take

$$\text{default: } \omega = 3 - \alpha, \quad (10)$$

and where not explicitly stated in plots, this will be the choice that we adopt.

IRC-safety subtleties connected with the large Δy_{ij} behaviour of normal ΔR_{ij}^2 distances are relevant for all flavour algorithms, though sometimes the issues appear only at orders beyond α_s^2 . Further discussion of this point is provided in Apps. B 1, C 1 and C 3. Note also that the

⁹ We have also explored the border case of $\alpha + \omega = 2$ and find that it diverges. This is relevant in particular to the case of $\alpha = 1$ and $\omega = 1$, for which u_{ik} coincides with the ik squared invariant mass when i and k are massless, i.e. a JADE-like distance [30, 31]. An issue to be aware of with an invariant-mass distance in a hadron collider context is that the invariant mass between an energetic initial-state collinear emission and a hard final-state particle is commensurate with that between two well separated hard final-state particles. Furthermore, a potential solution to this issue, i.e. clustering initial-state collinear emissions early, via their small invariant mass with the beam, involves ambiguities in the identification of the beam energy.

original formulation of the k_t algorithm for hadron colliders [4] foresaw the possibility of an angular distance Ω_{ik}^2 with $\omega = 1$, though this does not have IRC safety implications for the kinematic aspects of normal jet clustering.

D. Need for recursion

A key element of IFN is the recursion in step N4 above. The need for recursion can be illustrated with the help of Fig. 4. Again considering the anti- k_t or the C/A clustering algorithms, the first clustering step is that of particles 3 and 4. If $p_{t3} < p_{t4}$, their clustering triggers a flavour neutralisation search. That search will identify particle 2 (from a large-angle soft pair) as a potential neutralisation candidate. With $\alpha = 1$, we will have $u_{23} \ll u_{34}$, while for $\alpha = 2$, $u_{23} \sim u_{34}$. Either way, without recursion, it would be possible for 2 to neutralise the flavour of 3, which would ultimately result in the hard jet being flavourless. In the absence of the (1,2) pair, the hard jet would be flavoured. This would induce an infrared divergence.

The recursive aspect of the algorithm resolves this problem as follows: when 2 is identified as a neutralisation candidate for 3, the recursive search that is triggered in step N4 identifies particle 1 as a neutralisation candidate for 2. For both $\alpha = 1$ and $\alpha = 2$, we have $u_{12} \ll u_{23}$, and so particles 1 and 2 will neutralise. When the algorithm exits the recursion step, there are no longer any remaining flavoured particles to neutralise the flavour of particle 3. Thus the hard jet will retain its net flavour, resolving this IRC safety issue (see e.g. App. B 2).

E. Further comments

We conclude this section with a few general comments about the IFN algorithm.

A first comment concerns single parton consistency, as discussed in Sec. III. A potentially useful characteristic of IFN, shared with GHS, is that for configurations where each jet contains no more than one particle, the flavours of those jets are identical to those in standard anti- k_t . This is trivial, because for such configurations there is never a situation where two particles would cluster together and so the flavour neutralisation part of the algorithm is never triggered. Thus any leading-order jet calculation, for an arbitrary number of final-state jets, will give identical jets and flavours for those jets in the anti- k_t and its IFN extension.

A second comment concerns the fact that unlike the flavour- k_t algorithm, the flavour-related part of our IFN algorithm has no specific treatment of beam distances for flavoured particles (the CMP algorithm has similarities in that it leaves the anti- k_t beam-distance untouched for flavoured particles). This means that particular care is needed around the potential for long-distance clusterings,

as discussed in Sec. III C. Nevertheless, even algorithms with beam distances can suffer from long distance clustering when using standard ΔR_{ij}^2 type angular measures, as discussed in App. C 1.

A third comment concerns events with more than one flavour, e.g. both c and b flavour. One possibility is to consider all flavours within a single IFN run. Suppose i has flavour b and is about to cluster with j . This triggers a search for candidates to neutralise i 's flavour. The search may find a particle k with flavour $c\bar{b}$ (which could have arisen, for example, through earlier clusterings). The recursion of the IFN algorithm may then identify some other particle with flavour \bar{c} , which neutralises the c component of k 's flavour. Thus c flavour elsewhere in the event is affected by the b flavour in the $i + j$ clustering. Alternatively, one could choose to run the IFN algorithm first for the b flavour, then for the c flavour. In that case, the flavour neutralisation steps for b flavour have no side effects on those for c flavour. Consequently, the output of the algorithm can be different according to whether one runs it for all flavours at once, or separately a flavour at a time. In those of our studies below that include multiple flavours (the IRC safety tests of Sec. IV for the IFN algorithms, and the phenomenological study of Sec. V C), we treat all flavours at once.

In the discussion so far, we have always described the IFN algorithm as happening at the same time as the kinematic clustering. However, because IFN preserves the kinematic clustering sequence, the neutralisation steps can also be run as an add-on. Here, one loops again through each step of the kinematic clustering and updates the flavour information. This may be more convenient in cases where one already has a jet collection (and associated clustering sequence) defined.

A final comment concerns the “bland” option of flavour- k_t [1], which sets to infinity any clustering distances that would lead to flavours that are inconsistent with a single partonic flavour (e.g. bb or $c\bar{b}$).¹⁰ One could imagine a similar bland extension for our flavour neutralisation distances, but we leave the study of this question to future work.

IV. IRC SAFETY: DISCUSSION AND TESTS

Given the considerable subtlety of IRC safety for jet flavour, it is important to design tests to help build confidence in the IRC safety of any new algorithm. Subtle IRC-safety problems have arisen in the past in the context of cone-type jet algorithms, which ultimately led to the construction of an automated testing framework, used to verify the IRC safety of the SISCone algorithm [27]. Here we adapt and substantially extend that

¹⁰ This approach was adopted also in the IRC-unsafe “QCD-aware” clustering algorithm [29], without any clustering distance modification.

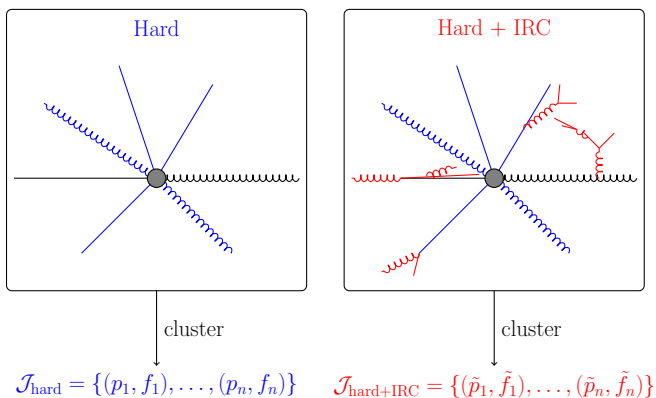


FIG. 5. On the left, hard particles (in blue) are generated, some with flavour, at central rapidities. The event is clustered with a given jet algorithm, resulting in a set of “hard” jets $\mathcal{J}_{\text{hard}} = \{(p_1, f_1), \dots, (p_n, f_n)\}$, with kinematics $\{p_i\}$ and associated flavours $\{f_i\}$. On the right, additional IRC radiation is added to the event as explained in the main text. This modified event is then clustered with the same jet algorithm, and the resulting set of “hard+IRC” jets $\mathcal{J}_{\text{hard+IRC}} = \{(\tilde{p}_1, \tilde{f}_1), \dots, (\tilde{p}_n, \tilde{f}_n)\}$ is compared against the original set of hard jets (and similarly for each hard step of the underlying clustering sequence). The sets agree if both the kinematics and the flavours of the various jets (and hard clustering steps) are identical. In the limit where the extra radiation becomes soft and collinear, the rate of failed events (where $\mathcal{J}_{\text{hard}} \neq \mathcal{J}_{\text{hard+IRC}}$) should go to zero for an algorithm that is IRC safe. The right-hand figure also serves to illustrate some of the classes of IRC additions that we make, though in practice we do not go beyond sixth order in α_s , i.e. we do not simultaneously add as many emissions as are shown.

framework. The framework is available on request from the authors.

A. Methodology

Our approach is illustrated in Fig. 5, which goes beyond the tests performed in the more recent literature. We begin by generating a random “hard” event, with some number of particles (flavoured or not), and run the clustering with the jet definition that we wish to test. This results in a set of hard jets, $\mathcal{J}_{\text{hard}} = \{(p_1, f_1), \dots, (p_n, f_n)\}$ with kinematics $\{p_1, \dots, p_n\}$ and associated flavours $\{f_1, \dots, f_n\}$. Note that here, we do not force the total 4-momentum (or even transverse momentum) of the hard event to be balanced, i.e. it is as if the events have neutrinos, leptons or isolated photons that would balance the momentum but do not take part in the clustering. We then construct a modified “hard+IRC” event, where we add soft emissions and collinear splittings up to some given order in α_s . We cluster that modified event and verify whether the hard jets in the modified event, $\mathcal{J}_{\text{hard+IRC}}$ coincide with the hard jets in the original event, both in terms of kinemat-

ics and flavour.¹¹ We then examine the rate of failure as a function of the logarithmic momentum range (L) of IRC additions. For an IRC-safe algorithm, we expect that failure rate to vanish as a (possibly fractional) power of the momentum scale of the IRC additions.

Ideally, we would consider all possible IRC insertions. There are two logarithms per order in α_s , and we have found that it is important to explore configurations at least up to α_s^4 . The smallest non-IRC-safe contribution would be a term independent of L , and at α_s^4 that would imply identifying one event in L^8 that fails. We will return to the question of the meaning and range of L below, but for now let us consider $L = 30$. That would imply identifying failures at the level of one event in $30^8 \simeq 6.6 \cdot 10^{11}$, which is prohibitive. Note, however, that the only contributions that give the maximum number of logarithms are those that exclusively involve the emission of simultaneously soft and collinear gluons, which are not the most likely configuration for triggering flavour-related IRC safety issues.

Consequently, we take a more targeted approach, in which we allow up to one logarithm per order in α_s , prioritising configurations that are potentially non-trivial from the point of view of flavour. We do so by omitting single soft-gluon divergences unless they involve a subsequent splitting to a pair of commensurate-angle partons.

B. Classes of IRC emissions

The specific IRC emissions included in our testing framework are shown in Fig. 6 and described below:

- **Final-state hard-collinear (FHC) emission:** we perform a (hard) collinear splitting of a randomly chosen final-state particle. We uniformly sample the logarithm of the transverse momentum of the splitting. We also uniformly sample the longitudinal momentum fraction of the splitting. This is consistent with our choice not to include the soft gluon emission divergence as part of the FHC class. For all flavour combinations ($q \rightarrow qg$, $g \rightarrow q\bar{q}$, $g \rightarrow gg$), an FHC branching is associated with one power of α_s and one logarithm of the IRC scale. For readers in the habit of using a Lund-diagram [34] representation of soft-collinear phase space, this corresponds to a strip close to the hard-collinear boundary in the Lund leaf of the emitter (Fig. 6a; that figure shows a shaded logarithmic transverse momentum range, which we further discuss below). Note that sensitivity to soft

¹¹ In the modified event, we also identify each step in the clustering sequence that involves clustering of two hard particles, and compare its kinematics and flavour to that of the corresponding step for the unmodified event.

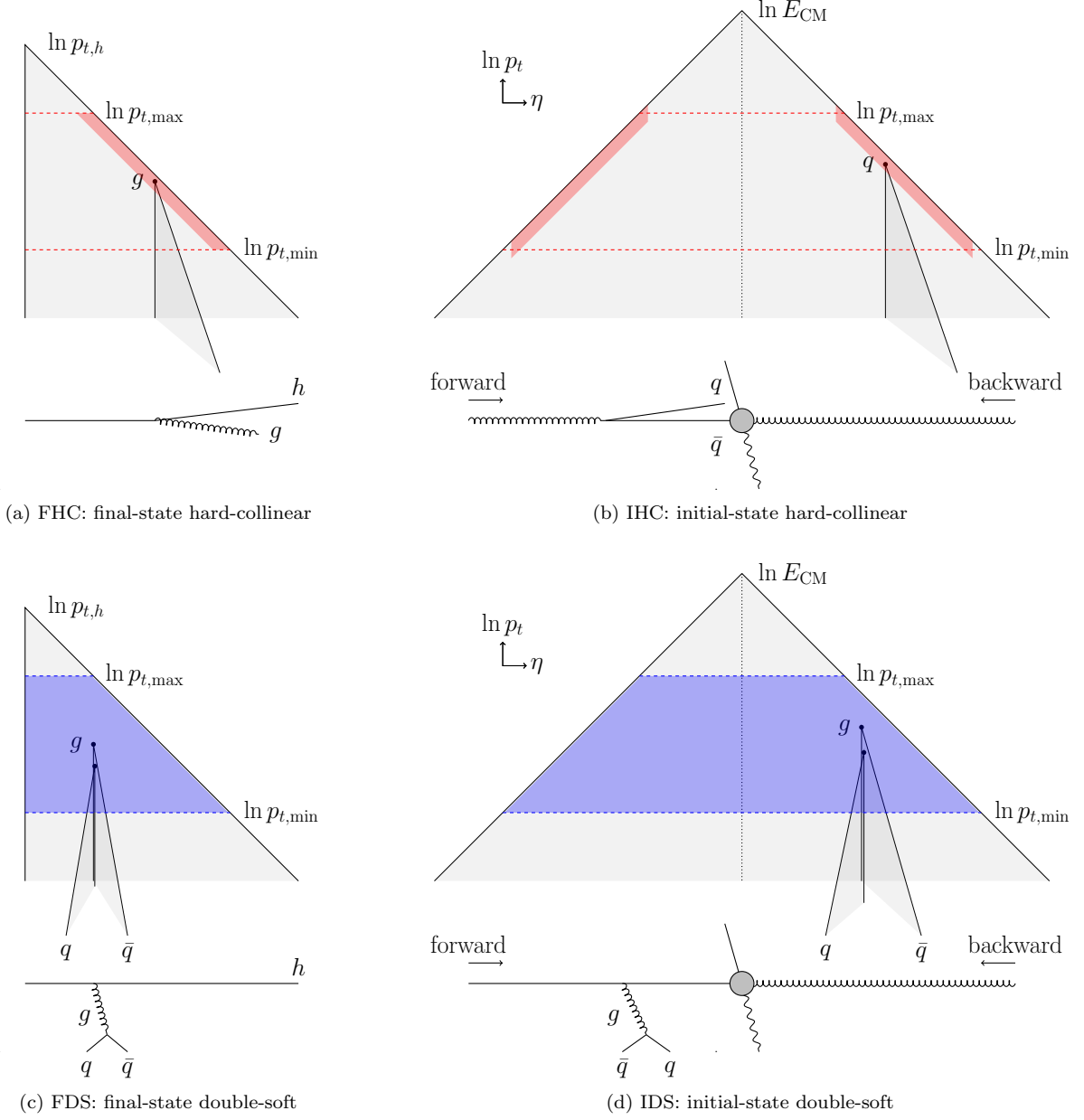


FIG. 6. Illustration of the emissions sampled in the “hard+IRC” event on a Lund diagram [34]. The left column shows emissions from a final-state jet. The right column shows initial-state radiation from the beams, where an emission collinear to the forward beam (coming from the left on the diagram) ends up at positive rapidities (right-hand half of the Lund plane), and vice-versa for an emission collinear to the backward beam. The top row shows hard-collinear splittings from (a, FHC) hard final-state particles or (b, IHC) the beams. The bottom row shows double-soft pairs, flavoured or not, being emitted from (c, FDS) hard final-state particles or (d, IDS) the beams. In a bin defined by $\ln p_{t,\min} < \ln p_t < \ln p_{t,\max}$, we sample any additional radiation in slices in the Lund planes (both for initial- and final-state radiation). We typically choose $\ln p_{t,\min} = 3 \ln p_{t,\max}$, with $\ln p_{t,\max} < 0$.

gluon emission will still be present in the analysis, but will be obtained through the double-soft (FDS/IDS) contributions below.

- **Initial-state hard-collinear (IHC) emission:** we perform a hard-collinear splitting of the beam (Fig. 6b). Again, we sample the longitudinal mo-

mentum fraction of the splitting uniformly, bringing one order of α_s and one logarithm.

- **Final-state double-soft (FDS) pair,** i.e. the addition of a $g \rightarrow gg$ or $g \rightarrow q\bar{q}$ pair. We choose one emitter randomly among the final-state hard particles, and uniformly sample the logarithm of

the transverse momentum $\ln p_{t,g}$ and the rapidity y_g of the intermediate gluon with respect to the emitter. This corresponds to uniform sampling of the bulk of the Lund leaf for that emitter (Fig. 6c) and brings one power of the coupling and two powers of the logarithm. We allow the intermediate gluon to split and distribute the kinematics of the resulting pair in such a way as to correctly reproduce the asymptotic behaviour of the $q\bar{q}$ double-soft matrix element in those kinematic regions where the splitting is asymmetric (either substantially different momentum fractions or rapidities, as elaborated upon in App. A). Note that even for $g \rightarrow gg$ splittings, we use the asymptotic matrix element for $g \rightarrow q\bar{q}$.¹² With the branching to a pair, we gain an extra power of the coupling and no logarithms, giving in total two powers of the coupling and two powers of the logarithm. We do not include the collinear divergence when $\theta_{q\bar{q}} \ll \theta_{hq} \sim \theta_{h\bar{q}}$, where h is the hard particle. That would bring three powers of logarithm for two powers of the coupling. That said, we still have configurations with $\theta_{q\bar{q}} \ll \theta_{hq}$, but those are generated by a different sequence, namely FDS production of a pair of soft gluons, followed by nested FHC branching of one of those gluons to a $q\bar{q}$ pair.

- **Initial-state double-soft (IDS) pair:** these are generated similarly to FDS, but with respect to the forward or backward beam (Fig. 6d). Note that both the IDS and FDS mechanisms include a subset of phase space where the double-soft pair is not collinear but instead at large angles, i.e. the configuration of Fig. 1. The matrix element for large-angle double-soft production is the same as collinear double-soft production (up to complications of colour factors), a consequence of longitudinal boost invariance of soft production in the (leading- N_c) colour dipole rest frame. As a result, the IDS component in particular is guaranteed to fully cover the soft large-angle double-soft phase space.

For each emission, we need to choose the range in $\ln p_t$, which we define as $\ln p_{t,\min} < \ln p_t < \ln p_{t,\max}$ (we choose our dimensions such that $\ln p_{t,\max}$ and $\ln p_{t,\min}$ are always

negative). One potential difficulty is that of proximity (or overlap) between the momentum scale of the IRC additions and the momentum scales of the hard event, because when there is proximity or overlap, the IRC additions can legitimately modify the hard event. If one keeps the range of hard scales fixed and takes IRC scales to zero, one expects the rate of such legitimate modifications to vanish. There should also be a suitably generous factor between the upper ($\ln p_{t,\max}$) and lower ($\ln p_{t,\min}$) edges of the IRC additions' $\ln p_t$ range, so as to be sensitive to IRC-unsafety mechanisms that work across a hierarchy of scales.

C. Implementation details

In our testing framework, the FHC, IHC, FDS, and IDS emissions are applied in a nested way (with some caveats, see below) so as to generate configurations up to order α_s^6 . We could have imposed angular ordering between nested emissions, but choose not to, so as to ensure that we retain sensitivity to cases where strict angular ordering might miss a potentially divergent part of phase space. We also allow for FHC emissions from the individual q , \bar{q} or g of the FDS and IDS pairs (again with no angular ordering condition).

Nesting is essential in order to test collinear splitting chains. It also partially alleviates worries of missing relevant IRC-unsafe configurations as a result of only considering configurations with one logarithm per power of the coupling. For example, as indicated above, $g \rightarrow q\bar{q}$ collinear splitting from a soft-collinear gluon ($\alpha_s^2 L^3$) is not generated directly, but the underlying L^3 divergence does appear in our framework, in the context of FDS (double gluon) emission followed by the nested collinear splitting of one of the soft gluons to $q\bar{q}$. This is not exactly the same configuration as the $\alpha_s^2 L^3$ divergence, since it involves an extra soft gluon. In effect, if there is a problem in an $\alpha_s^2 L^3 h \rightarrow hg \rightarrow hq\bar{q}$ configuration, we are making the assumption that we will still detect it in at least some of the $h \rightarrow hgg \rightarrow hqq\bar{q}$ configurations. For technical reasons, there are some nestings that we are missing: (a) nesting of one double-soft emission from a prior double-soft emission; and (b) insertion of double-soft emissions on more than one of the descendants of a collinear splitting. These limitations may be addressed in future work.

One final potential concern is that by allowing strongly angular-disordered configurations, we might mistakenly declare an algorithm to be IRC unsafe. To guard against that risk, when we identify an IRC-unsafe configuration, we further investigate it to establish whether it is genuine. All IRC failure classes that we identified were genuine, as documented in App. C.

We close this description with some final technical details:

- We generate a random number of hard particles, and randomly sample their flavours. The maxi-

¹² This might seem surprising at first sight, since the production of a soft gg pair has a qualitatively different structure from that of a soft $q\bar{q}$ pair when the pair is well separated. For example, for emission of a double soft gluon pair from a quark line, the component with the C_F^2 colour factor corresponds to independent emission, with logarithmic divergences both in the ratio of the gluon transverse momenta and the rapidity separation. However these contributions would be associated with the double (soft-collinear) logarithms that we are deliberately leaving out. Similarly the soft singularity in the $C_F C_A$ term would also bring an extra soft-gluon logarithm that is beyond what we aim to sample.

imum number of hard particles we consider is 8. In the figures targeting specific IRC-unsafe configurations, the hard particles' momenta are chosen randomly uniformly between 100 GeV and 1 TeV, and their rapidities uniformly in the range $|y| < 1.5$. In our final IRC safety tests for the IFN algorithms, we use a broader range, with the hard particles' momenta chosen randomly uniformly between 1 GeV and 1 TeV, and their rapidities taken uniformly within $|y| < 2.5$. Plots with results will always indicate the ranges used.

- The $\ln p_{t,\max}$ scale is typically scanned in the range -3 down to -42.5 (with p_t expressed in units of GeV). When we show a failure rate it will always include the $\ln^n p_{t,\max}/p_{t,\min}$ measure that arises from the n logarithmic integrations at a given order n , but it will not include overall constants such as colour factors. We will refer to this as a phase-space weighted failure rate.
- We generally use $\ln p_{t,\min} = 3 \ln p_{t,\max}$. However, in the tests of our IFN algorithms, we have also carried out a subset of tests with a larger ratio $\ln p_{t,\min} = 5 \ln p_{t,\max}$. Results are consistent between the two sets of tests.
- The jet radius is sampled randomly between 0.3 and 1.57.
- The jet algorithms are coded as plugins to FastJet [35] version 3.4.1 using techniques that allow for more accurate handling of large rapidities and very small rapidities. Ultimately, however, we found that in order to fully explore the phase space it was also necessary to use higher-precision numerical types from the `qd` package [36], up to four times normal double precision. This was achieved with the help of a suitably converted version of the `fjcore` form of the FastJet package. Many of the techniques that we explored were inspired by, adapted from and sometimes fed back to the PanScales project [26, 37, 38].
- In practice, the framework can operate in two modes: it can sample randomly across the available configurations at any given order, which is useful to systematically check whether there are any IRC-unsafe configurations for a given algorithm; alternatively, it can focus on a specific class of configuration, which is useful when trying to understand the detailed nature of any IRC safety issues that have appeared.
- For flavour jet algorithms where the flavour of the cluster sequence is meaningful (i.e. all algorithms except GHS), we test not just the flavour and kinematics of the final jets, but additionally those of all steps in the hard+IRC clustering sequence that correspond to steps in the hard clustering sequence.

- Some algorithms (such as flavour- k_t and IFN) can naturally handle multiple flavours at a time, while others (such as CMP and GHS) are designed around a single flavour at a time. Most of our tests will be carried out with one flavour. For the higher-order IFN tests that go into our summary, Table I, we use six light flavours, so as to ensure that we do not accidentally miss IRC issues that would arise only for multi-flavoured configurations. Plots will always be labelled with the number of light flavours used.

D. Results

Sample results from our numerical IRC-safety tests are illustrated in Fig. 7. The left-hand plot shows the α_s^2 FDS contribution to the phase-space weighted failure rate for the plain anti- k_t algorithm. The failure rate grows linearly with $\ln p_{t,\max}$, consistent with the expectation of an $\alpha_s^2 L$ divergence.

The middle plot of Fig. 7 shows the phase-space weighted failure rate for the anti- k_t +IFN algorithm (both with $\alpha = 1$ and $\alpha = 2$) at order α_s^2 . These results are summed over all sampled configurations (IDS, FDS, IHC², FHC², IHC×FHC). One sees that the failure rate vanishes as $p_{t,\max} \rightarrow 0$, consistently with a power law, implying no IRC divergence. The right-hand plot shows the results for anti- k_t +IFN at order α_s^4 . Again the plot indicates that the phase-space weighted failure rate vanishes as $p_{t,\max}$ is reduced, consistently with a power law.

For more negative values of $\ln p_{t,\max}$, no points are shown simply because we observed no failures with anti- k_t +IFN. The grey band at the bottom of the plots shows how the test is broken up into different regions with the number of events used for each region (5×10^9 in the lowest region). The regions each involve a different underlying numerical precision type in the code, and one of the limiting factors in our tests is the speed of the code in the lowest region where we are using four times the precision of a standard IEEE double type.¹³ Overall, the

¹³ In interpreting these results, one should keep in mind that the integration volume at order α_s^n is effectively $(\ln p_{t,\max} - \ln p_{t,\min})^n$. Defining $\ln p_{t,\max} \equiv L$ and $\ln p_{t,\min} = (1+c)L$ ($c = 2$ in Fig. 7), that corresponds to $(cL)^n$. Assuming that the failure rate for a L^p divergence goes as $(cL)^p$, then with N events in a given bin, we expect to observe a non-zero failure rate down to $L \sim -N^{1/(n-p)}/c$. Fig. 7 was generated with $N \sim 10^9$ events per point and $c = 2$. We therefore expect that up to $n = 4$ we should observe all main classes of failure (i.e. any case with $p \geq 0$) for $L \gtrsim -90$, i.e. over the full range of $L = \ln p_{t,\max}$ in Fig. 7 (keeping in mind that order 1 factors that we have neglected can have a significant impact on the range). For $n = 5$, failures with a $p = 0$ structure would be observed only for $L \gtrsim -30$, while for $n = 6$, this would reduce to $L \gtrsim -15$. Note that it is still useful to explore the full range of L , even at high orders n , because there can be cases where an IRC divergence appears for the first time already with some number of logarithmic en-

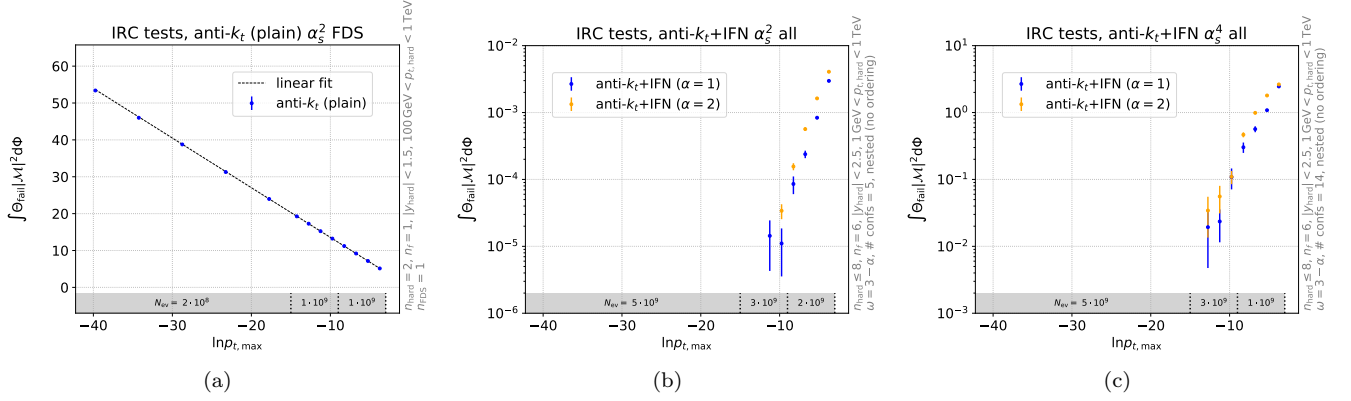


FIG. 7. Example results from our numerical IRC safety tests showing (a) the IRC unsafety of standard anti- k_t at order α_s^2 , and (b,c) the IRC safety of anti- k_t with Interleaved Flavour Neutralisation (IFN) at orders α_s^2 and α_s^4 , respectively. In all plots, the phase-space weighted failure rate is shown as a function of the maximum hardness of the extra radiation $\ln p_{t,\max}$, where we sample values $3 \ln p_{t,\max} < \ln p_t < \ln p_{t,\max}$ for any bin of $\ln p_{t,\max}$. In (a), the integrated failure rate is plotted on a linear scale for standard anti- k_t in the FDS configuration from Fig. 1 with one double-soft pair and 2 hard particles in the event. The classic anti- k_t IRC safety issue is confirmed numerically by the linear divergence $\alpha_s^2 \ln p_{t,\max}$, from one soft gluon splitting to a flavoured pair at large angle. In (b) and (c), the integrated failure rate is plotted on a logarithmic scale for anti- k_t with IFN for parameters $(\alpha = 1, \omega = 2)$ and $(\alpha = 2, \omega = 1)$, for all configurations that contribute at (b) order α_s^2 and (c) order α_s^4 , with up to 8 hard particles in the event and up to 6 flavours. The total failure rate goes to zero as $\ln p_{t,\max} \rightarrow -\infty$, implying the IRC safety of anti- k_t with IFN to the tested order and accuracy. The absence of points below $\ln p_{t,\max} \simeq -15$ signals no IRC safety failures out of the $5 \cdot 10^9$ events studied for lower $\ln p_{t,\max}$ values (the number of events in each of three regions of $\ln p_{t,\max}$ is indicated in the shaded bands at the bottom of the plot). The plots also include moderately small values of $\ln p_{t,\max}$ so as to better show the overall scaling behaviour.

results provide a strong indication of IRC safety for the anti- k_t +IFN algorithm developed in this paper.

Table I summarises the results of our testing framework applied to a range of jet algorithms. At lowest order, we organise the results according to the class of divergence being probed, as indicated in the second column of the table, while at higher orders we limit the breakdown to configurations that have turned out to be of specific interest. The corresponding failure rate plots for the IFN algorithms (with the anti- k_t and C/A algorithms) are given in App. D.

Algorithms whose failure rate goes down as the extra radiation becomes softer/more collinear are indicated by a checkmark (✓). Algorithms that develop a divergence (a non-vanishing integrated failure rate as $\ln p_{t,\max} \rightarrow -\infty$) for a given target configuration, are marked by a red cross (✗). For each case that has shown a divergence, we have examined a few events where there is a clear failure and developed an analytic understanding of the nature of the problem. We will briefly discuss each issue here, while the table also links to the relevant part of App. C with further analytic and numerical studies.

The first two rows of Table I emphasise that at order α_s with just one emission (FHC or IHC), there are no divergences for any jet algorithm with IRC safe kinematics, even without a special treatment of flavour. The classic IRC safety problem of standard anti- k_t only shows up at order α_s^2 , as highlighted in the next two rows of Table I for a configuration with one double-soft pair (see Fig. 1). That problem arises in both the FDS and the IDS channels, and in each case it appears for the subset of events where the FDS or IDS pair is at large angles. From the table, it is clear that all flavour jet algorithms solve that original IRC safety issue.

However, the tests reveal new issues for all algorithms other than our IFN-based procedure. In two cases, flavour- $k_{t,\Omega}$ and CMP_Ω , we will propose modifications that seem to resolve the problem(s). For the interested reader, the summary of the issues is as follows:

- **Initial-state (IHC×IDS) subtlety at α_s^3 for flavour- k_t and GHS.** The “ \sim ” for $\alpha = 2$ flavour- k_t and GHS at α_s^3 (IHC×IDS) indicates a borderline case. It arises, for example, for a hard event consisting of a single energetic parton (and resulting hard jet), supplemented with a hard-collinear initial-state splitting and a large-angle double-soft pair, which may be IDS or FDS (see Fig. 15, together with the complete details in App. C1). When one (anti)quark from the double-soft pair is somewhat softer than the other, its d_{ij} distance with the hard-collinear particle can be smaller than that with the other (anti)quark from the soft pair,

hancements (e.g. the L^3 divergence that appears at α_s^4 in the GHS algorithm, as discussed in App. C5). A final comment concerns the overall normalisation of the result of the phase-space weighted failure rate. This can appear large at moderate values of L where there are still failures, because it includes the $(cL)^n$ integration volume.

order relative to Born		anti- k_t	flav- k_t ($\alpha = 2$)	CMP	GHS $_{\alpha,\beta}$ (2, 2)	anti- k_t +IFN $_{\alpha}$	C/A+IFN $_{\alpha}$
α_s	FHC	✓	✓	✓	✓	✓	✓
	IHC	✓	✓	✓	✓	✓	✓
α_s^2	FDS	✗ II B	✓	✓	✓	✓	✓
	IDS	✗ II B	✓	✓	✓	✓	✓
	FHC×IHC	✓	✓	✓	✓	✓	✓
	IHC ²	✓	✓	✗ C 2	✓	✓	✓
	FHC ²	✓	✓	✓	✗ C 4	✓	✓
α_s^3	IHC×IDS		~C 1	✗ C 3	~C 1	✓	✓
	rest					✓	✓
α_s^4	IDS×FDS				✗ C 5	✓	✓
	rest					✓	✓
α_s^5						✓	✓
α_s^6						✓	✓

TABLE I. Summary of the IRC safety test results. Red crosses (✗) indicate a clear failure of IRC safety. Checkmarks (✓) signify that the algorithm passes numerical tests at that order or for that configuration. The tilde (∼) for flavour- k_t (and by extension GHS, which uses flavour- k_t distances) indicates marginal convergence, though one expects divergent behaviour at higher orders. For algorithms that fail or are marginal at a given order, we display greyed-out boxes at higher orders, since those higher orders are also bound to fail. In a few cases, we have identified a new class of problem that only arises at higher order and we explicitly mark these with a red cross. The GHS parameters here are set to $\alpha = 2, \beta = 2$. The IFN procedure is tested both for the anti- k_t and C/A algorithms, and the IFN parameters are chosen as $\alpha \in \{1, 2\}$ with $\omega = 3 - \alpha$ (tests are successful for both sets of parameters). Detailed discussions of the issues identified are linked to from the relevant table cells. Plots in support of the IRC safety conclusion for the IFN combinations are to be found in App. D, specifically Figs. 24 and 25, as are plots (Figs. 26 and 27) supporting the IRC safety of our modified versions of the flavour- k_t and CMP algorithms, respectively flavour- $k_{t,\Omega}$ and CMP $_{\Omega}$, which are discussed in the text. (They are not shown in the table, because we have run them with lower statistics.)

essentially because the ΔR_{ij}^2 distance goes as Δy_{ij}^2 , which is only logarithmically large. The large-angle soft (anti)quark and the initial-state collinear quark cluster, leaving a lone large-angle soft quark, which can contaminate the flavour of the hard jet. At $\mathcal{O}(\alpha_s^3)$ one ends up with an integral that goes as $\int d \ln p_t / (\ln p_t)^2$. This integral converges for $p_t \rightarrow 0$, however the way in which the integrand (multiplying $d \ln p_t$) vanishes as $p_t \rightarrow 0$ is not a power-law in p_t . One may thus consider the algorithm to be marginally safe at this order, however at the next order one would expect to see additional logarithmic enhancements. These might arise, e.g. from the running of the QCD coupling or evolution of the parton distribution functions (PDF), and would ultimately cause the integral to diverge. Indeed, our study identified a problem in the IHC²×IDS channel at order α_s^4 . However, a conclusive understanding of this configuration requires inclusion also of the virtual and PDF-counterterm contributions, which is beyond the scope of this study. A similar problem arises with $\alpha = 1$, but with extra logarithms in the denominator of the corresponding integral. This generic class of problem can be solved by replacing $\Delta R_{ij}^2 \rightarrow \Omega_{ij}^2$, and, as before, we will use Eq. (10) as our default choice for its ω parameter. We refer to the modified algorithm as flavour- $k_{t,\Omega}$. This simple adaptation is possible because the issue is not with the original underlying

strategy, but rather with the subtleties that arise in distance measures with QCD initial-state radiation (the same comment holds for related issues in other algorithms). As a consequence we do not expect to have to make any modifications to the e^+e^- version of the flavour- k_t algorithm.

- **Initial-state (IHC²) issue at α_s^2 for CMP.** This issue arises, for example, for a hard (Born) event consisting of a single hard parton, supplemented with two collinear initial-state quark and anti-quark emissions, one on each beam (see Fig. 17 and App. C 2). Those initial-state emissions cluster in the first step of the algorithm, producing a large-mass, low- p_t flavourless pseudojet at central rapidities, which can then cluster with the hard parton, modifying its kinematics. The problem arises because in the CMP distance Eq. (4), the small factor from the transverse-momenta dominates over the (only logarithmically large) factor from the rapidity separation between the pair. Ultimately this leads to an $\alpha_s^2 L^2$ divergence. It can be resolved by replacing

$$\mathcal{S}_{ij} \rightarrow \bar{\mathcal{S}}_{ij} = \mathcal{S}_{ij} \frac{\Omega_{ij}^2}{\Delta R_{ij}^2} \quad (11)$$

for oppositely flavoured pairs and requiring the parameter $\omega > 1$ in the Ω_{ij} distance. In practice, we find that this modification has almost no impact on

the phenomenological behaviour of the algorithm (e.g. $\lesssim 1\%$ in Fig. 9 below). We refer to this modified version of the CMP algorithm as CMP_Ω and unless otherwise specified we use $\omega = 2$.

- **Initial-state (IHC \times IDS) issue at α_s^3 for CMP.** This issue involves the same configuration and sequence that led to a marginal issue for flavour- k_t (Fig. 15), but here it brings an $\alpha_s^3 L$ divergence (App. C 3), rather than α_s^3/L . Recall that the problem here is that the quark from the large-angle double-soft pair can cluster with the IHC (\bar{q}) particle, leaving the large-angle soft \bar{q} to contaminate the hard jet flavour. The different IRC behaviour of CMP versus flavour- k_t can in part be attributed to the fact that the CMP algorithm retains the standard anti- k_t form of the beam distance, causing the beam-clustering of the IHC particle to come at the end of the algorithm. In contrast, in the flavour- k_t algorithm, the IHC beam clustering nearly always comes before the IHC particle can cluster with the soft large-angle quark, reducing the phase-space associated with IRC problems for this configuration. The fix of Eq. (11), i.e. CMP_Ω , also solves this problem.
- **Final-state (FHC 2) issue at α_s^2 for GHS.** This problem appears with four hard particles such that each of two hard jets contains one flavoured (q or \bar{q}) and one non-flavoured particle, as could arise in semi-leptonic $t\bar{t}$ decays when considering only b 's to be flavoured. The α_s^2 modification of the event involves the hard-collinear splitting of one of the energetic quarks, followed by the hard-collinear splitting of that gluon into a $q'\bar{q}'$ pair (see Fig. 20 and App. C 4). The accumulation stage leaves the collinear $q'\bar{q}'$ as separate flavour clusters, and relative to the original Born event, the energy of the hard q 's cluster is modified. During the dressing stage, the collinear $q'\bar{q}'$ annihilate immediately, but the modification of the energy of the hard- q cluster means that that cluster can behave differently during the dressing stage. We envisage that this problem could be solved by accounting for energies within each jet during the dressing stage, but have yet to formulate a concrete modification of the algorithm. This issue is present independently of the parameters of the algorithm and leads to an $\alpha_s^2 L^2$ divergence.
- **Mixed initial/final-state (IDS \times FDS) issue at α_s^4 for GHS.** This problem involves a hard event with one Born gluon (h) leading to a single hard jet.¹⁴ The issue arises with a final-state

soft-collinear $q_1\bar{q}_2$ pair emitted inside the jet and a large-angle $q_3\bar{q}_4$ pair (see Fig. 22 and App. C 5). If $\theta_{h1} < \theta_{12}, \theta_{h2}$, then the $h1$ clustering will be the first step of the accumulation stage and may pass the SoftDrop condition, resulting in a pseudojet with the energy of h but the flavour of 1, which goes on to form a flavour cluster separate from that of q_2 . The two flavour clusters in the jet now have a large hierarchy of energy, and the softer one (q_2) may ultimately annihilate with a large-angle soft quark (3 or 4) if the latter has a similar (or larger) p_t with respect to the beam, resulting in the flavour of the hard jet being set by the $h1$ cluster. This issue gives an $\alpha_s^4 L^3$ divergence for $\alpha\beta > 2$, and numerical results are consistent with an $\alpha_s^4 L$ divergence for $\alpha\beta = 2$. The analytical study of App. C 5 indicates that the problem should be resolved when one takes $\alpha\beta < 2$ (if one additionally replaces $\Delta R_{ij}^2 \rightarrow \Omega_{ij}^2$), though the above FHC 2 issue remains.

The discovery of the above issues highlights the importance of having a systematic framework for testing IRC safety. Indeed, some of these issues were first discovered with the testing framework, as were the identification of $\alpha\beta < 2$ as a potential solution for the GHS α_s^4 (IDS \times FDS) issue, and the requirement Eq. (9) for the IFN algorithm. Such tests also led us to suspend study of more general u_{ij} distances involving $u_{ij} = [\max(p_{ti}, p_{tj})]^{2p} [\min(p_{ti}, p_{tj})]^{2q} \Omega_{ij}^2$, specifically a dimensionless form with $p = -q = 1$.

A final comment is that it is important to remember that the IRC tests cover many cases, but are not totally exhaustive. Specifically, as discussed in Sec. IV A, we have at most one power of L per power of α_s , and only up to α_s^6 , the events that we have generated have a band gap,¹⁵ and a couple of nestings are still missing, notably as regards double-soft emissions. Thus our tests should not be considered an ultimate proof of IRC safety, but merely a strong indication.

V. PHENOMENOLOGICAL ILLUSTRATIONS

In this section, we present three phenomenological test cases, intended to convey some of the main features of

¹⁴ We are grateful to Simone Marzani for discussions that first led us to investigate this configuration analytically.

¹⁵ By band gap we mean the white region between the upper hard tip of the Lund diagrams in Fig. 6 and the upper edge of the shaded region. The concern that one might have is that of an IRC unsafety mechanism whereby an emission at some momentum scale ϵ clusters with an emission at a still soft, but much larger scale $\epsilon^{1/p}$ (for some $p > 1$) in the white band-gap region, and only after that clustering can it cause the IRC unsafety. Our test procedure is only sensitive to values of $p < \ln p_{t,\min}/\ln p_{t,\max}$. One would therefore like to take as large a value of that ratio as possible, keeping in mind however that larger values of $\ln p_{t,\min}/\ln p_{t,\max}$ are numerically more challenging, both because of the higher precision and the need for higher statistics, cf. footnote 13.

our IFN algorithms. We include comparisons to standard anti- k_t clustering and also to those prior flavour algorithms for which we have been able to identify an IRC-safe adaptation, namely flavour- $k_{t,\Omega}$ and CMP $_{\Omega}$.

The first two tests will be specific to heavy flavour, which is the main experimental application of flavoured jet algorithms. The third test will be for generic flavour and can be seen as a stress test of the algorithm's practical performance with light flavour at parton level.

A. Heavy flavour in $pp \rightarrow WH(\rightarrow \mu\nu b\bar{b})$

We begin with the case of Higgs production in association with a W boson at hadron colliders, $pp \rightarrow WH$, where the Higgs boson decays to a pair of b -quarks and the W decays leptonically. This process is of interest for obvious phenomenological reasons, e.g. because of the sensitivity to the HWW and $Hb\bar{b}$ couplings, and it has been measured by both ATLAS and CMS [39, 40]. Additionally, it is one of the processes in which one can probe high- p_t Higgs production [41, 42], especially in conjunction with jet substructure tools [43, 44], bringing particular sensitivity to new physics. For a long time, calculations at NNLO QCD were performed with massless b quarks, which prohibited the use of the standard anti- k_t algorithm to cluster the final state. Only recently [32] was the calculation performed with massive b -quarks.

Here, we examine a classic resolved-jet analysis of this process, similar to that of Ref. [32]. We use Pythia 8.306 [45, 46] with the 4C tune [47] to generate $pp \rightarrow W(\rightarrow \mu\nu_{\mu})H(\rightarrow b\bar{b})$. Following Ref. [32], we require the presence of a muon satisfying

$$|\eta_{\mu}| < 2.5, \quad p_{t\mu} > 15 \text{ GeV}. \quad (12a)$$

We cluster the event with a given jet algorithm, using a jet radius of $R = 0.4$, and identify b -flavoured jets that satisfy

$$|y_{j_b}| < 2.5, \quad p_{tj_b} > 25 \text{ GeV}. \quad (12b)$$

We require the event to have at least two such jets. Finally, the reconstructed Higgs boson is defined as the 4-momentum sum of the two b -jets whose invariant mass is closest to the Higgs mass.

The distribution of the transverse momentum of the reconstructed Higgs boson is presented in Fig. 8 at hadron level (with multi-parton interactions turned on), for four algorithms:

- standard anti- k_t with net flavour summation (red),
- anti- k_t with our IFN algorithm ($\alpha = 2$, in green),
- the CMP $_{\Omega}$ algorithm ($a = 0.1$, where the angular part of the distance measure is corrected as in Eq. (11), in black), and
- the flavour- $k_{t,\Omega}$ algorithm ($\alpha = 2$, in gold).

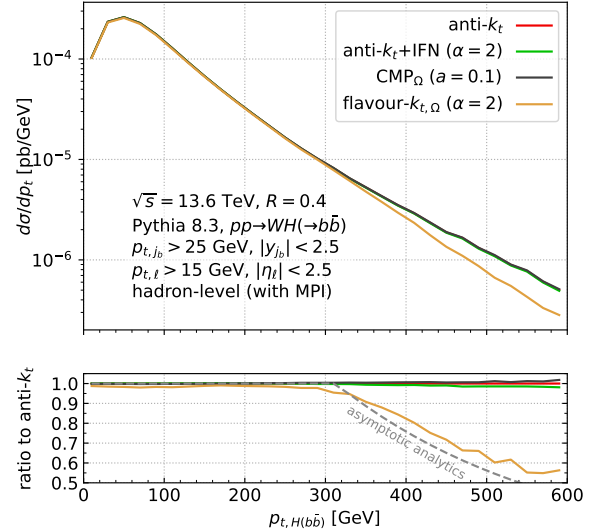


FIG. 8. The transverse momentum spectrum of the reconstructed Higgs boson in $WH(\rightarrow \mu\nu b\bar{b})$ at centre-of-mass energy $\sqrt{s} = 13.6$ TeV, at hadron level (with stable B -hadrons). The upper panel shows the spectrum for four jet algorithms: anti- k_t with net flavour of the jet constituents (red), our IFN version of anti- k_t (with $\alpha = 2$, green), the CMP $_{\Omega}$ algorithm (as adapted from Ref. [10] with a fix of the angular measure, see Eq. (11), black) and the flavour- $k_{t,\Omega}$ algorithm (with $\alpha = 2$, gold). The lower panel shows the ratio to standard anti- k_t . CMP $_{\Omega}$ and our IFN algorithms all give very similar results to those from the plain anti- k_t algorithm. In contrast, as already pointed out in Ref. [32], flavour- $k_{t,\Omega}$ jets can differ significantly from anti- k_t kinematics at large transverse momentum, because they start clustering the b and \bar{b} together into a single jet well before the scale of $p_t \simeq 2m_H/R = 625$ GeV where this occurs with the normal anti- k_t algorithm. This is reflected in Eq. (13c), which is used to generate the “asymptotic analytics” curve in the lower panel.

The flavour- $k_{t,\Omega}$ algorithm leads to a reconstructed Higgs spectrum that is markedly different from that of the anti- k_t algorithm. In particular, for $p_{tH} \gtrsim 300$ GeV, the distribution starts to drop relative to that with anti- k_t , reaching about 60% of the latter's value at $p_{tH} \sim 600$ GeV. As noted in Ref. [32], this occurs because the flavour- k_t algorithm starts clustering the b and \bar{b} together at lower values of p_{tH} than for the anti- k_t algorithm. When the b and \bar{b} end up in a single jet, the event fails the selection requirement of having at least two b -jets. Specifically for the decay of a scalar particle with invariant mass m and transverse momentum p_t , for small R and in the limit of $p_t R \ll m$, the efficiency for having two separate jets (without any p_t or rapidity cut on the jets) is 1 at low p_t . Above some threshold in $x = p_t R/m > x_{\min}$,

it becomes

$$\text{gen-}k_t : \quad 1 - \frac{\sqrt{x^2 - 4}}{x}, \quad x_{\min} = 2, \quad (13a)$$

$$\alpha = 1 \text{ flav-}k_t : \quad \frac{2}{x^2}, \quad x_{\min} = \sqrt{2}, \quad (13b)$$

$$\alpha = 2 \text{ flav-}k_t : \quad \frac{2}{1 + x^2}, \quad x_{\min} = 1. \quad (13c)$$

The last of these, in particular, explains the qualitative behaviour seen in Fig. 8, cf. the “asymptotic analytics” dashed line in the lower panel. Note that Eqs. (13b) and (13c) are independent of the $\Delta R_{ij}^2 \rightarrow \Omega_{ij}^2$ change, because they are evaluated in a small-angle limit, where the two distance measures are identical.

In Fig. 8, the CMP_Ω algorithm, as well as anti- k_t +IFN, give results that are very similar to those of plain anti- k_t jets, to within about a percent. This result is not entirely trivial: while it was expected that the new generation of flavour algorithms should be kinematically more similar or identical to anti- k_t , there was still a possibility that flavour assignments could modify cross sections, e.g. because the original anti- k_t jets’ flavours would have been subject to modifications from soft $b\bar{b}$ pairs, while any such effect should be substantially reduced for the new algorithms. The absence of a numerically significant difference between jet algorithms other than flavour- $k_{t,\Omega}$ suggests that for signal processes like that shown here, with $R = 0.4$ jets, the contribution of soft $g \rightarrow b\bar{b}$ contamination is relatively small. On one hand, this means that certain experimental signal measurements with standard anti- k_t jets may not require much unfolding in order to be compared to the flavoured jet definitions. On the other hand, if one is to perform a higher-order calculation with the approximation of massless b quarks, a flavoured jet algorithm will still be required in order to obtain a finite result.

B. Heavy flavour in $pp \rightarrow t\bar{t} \rightarrow \ell\nu + \text{jets}$

For our second test case with heavy flavour, we consider top-quark pair production in hadron collisions with semileptonic top decays $pp \rightarrow t\bar{t} \rightarrow \ell + \text{jets}$. We select events by requiring at least one muon with

$$p_{t\mu} > 30 \text{ GeV}, \quad |\eta_\mu| < 2.4, \quad (14)$$

and additionally $p_{t,\text{miss}} > 30 \text{ GeV}$. We then run a jet algorithm and examine the p_t distribution of jets that are considered b -flavoured according to a given jet algorithm, with a requirement of $p_t > 20 \text{ GeV}$ applied to the jets. We again use Pythia 8.306, but now with the Monash13 tune [48]. It will be instructive to examine results at both tree-level (where we use b quarks as the flavoured inputs to the algorithms) and hadron level including parton showering (where we use stable B -hadrons as the flavoured inputs).

The results are shown in Fig. 9. The inclusive b -jet p_t spectrum is shown in the upper panels, on the left at

partonic tree level, i.e. without shower or hadronisation, and on the right at hadron level including showering. We examine the same algorithms as in Fig. 8 and since we are again interested in the similarity of the distributions to that of standard anti- k_t with net flavour summation (in red), the lower panels show the ratio to that result. Additionally, we include a line for standard anti- k_t clustering with “any-flavour” tagging, i.e. counting a $b\bar{b}$ -jet as a b -tagged jet, which is more in line with experimental procedures than net flavour recombination.

Let us start by examining the tree-level results in Fig. 9a. When each jet contains at most one parton, the IFN algorithm is, by design, intended to give identical results to the plain net-flavour anti- k_t algorithm. Note that the tree-level Pythia sample does not guarantee this property, since our analysis does not require each of the four tree-level partons to be in four separate jets and, sometimes, two tree-level partons may cluster together. Nevertheless, we see that the IFN algorithm (green) gives results that are essentially indistinguishable from the plain net-flavour anti- k_t net-flavour (red) results. The flavour- $k_{t,\Omega}$ algorithm (gold) is expected to show differences, but these are relatively modest, typically a few percent. Finally the CMP_Ω results (with $a = 0.1$, including the IRC fix as in Eq. (11), in black) show a few-percent depletion of low- p_t b -jets. We believe that this is a consequence of the small clustering distance for pairs of two low- p_t b -flavoured particles, which enhances the likelihood that such pairs will cluster, even when well separated.

At hadron-level in Fig. 9b, including parton showering and multi-parton interactions, the qualitative pattern is broadly similar, but with some effects enhanced relative to what is seen at tree level. Now there are very small differences between anti- k_t and IFN, below a percent — this once again suggests that soft $g \rightarrow b\bar{b}$ induced contamination is a small effect, as we noted in the WH case of Sec. V A. In contrast, the relative differences of flavour- $k_{t,\Omega}$ and CMP_Ω as compared to anti- k_t now reach 8–10%. Further examining the results we have identified two effects that contribute to this: (1) a small reduction of the ratios due the shower and hadronisation, in events where there are two B -hadrons, perhaps because fragmentation of the b quarks enhances the impact of modified clustering distances for flavoured particles; and (2) substantially smaller ratios, especially at low p_t , in the $\sim 8\%$ of events with an additional $b\bar{b}$ pair from the showering.

Finally, regarding anti- k_t with “any-flavour” recombination (in blue), we see that it differs only by a few percent from the net-flavour tagging and the IFN algorithms. The difference appears mostly to be associated with events where the b and \bar{b} from the t and \bar{t} decays end up in a single jet. Insofar as any-flavour recombination is a good stand-in for standard experimental tagging, the similarity of net-flavour and any-flavour recombination indicates only a limited need for unfolding corrections in order for experimental $t\bar{t}$ results to be presented unfolded to an IFN-style flavour truth level. Note, nevertheless,

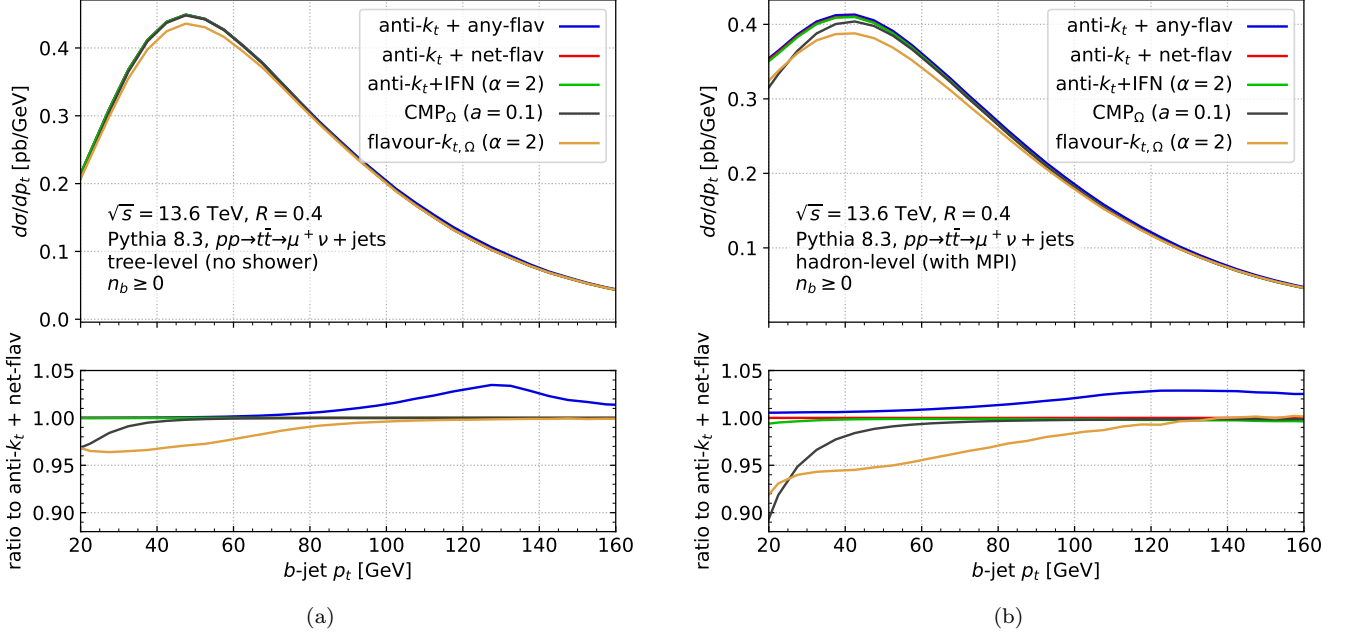


FIG. 9. Inclusive b -jet spectrum from Pythia 8.3 in $pp \rightarrow t\bar{t} + X \rightarrow b\mu^+ \nu \bar{b}q\bar{q}' + X$ events at $\sqrt{s} = 13.6$ TeV, at (a) partonic tree level (i.e. no showering or hadronisation) and (b) hadron level (with stable B -hadrons). The distribution is shown in the upper panels, for four jet algorithms (as in Fig. 8) and additionally for anti- k_t with “any-flavour” recombination (i.e. a $b\bar{b}$ jet counts as b -tagged). The lower panels show the ratio to anti- k_t jets with net flavour summation. The anti- k_t +IFN algorithm yields a b -jet spectrum that is almost identical to that from the net-flavour anti- k_t algorithm, across the whole p_t range. The closeness to anti- k_t holds both at tree level and after showering and hadronisation (with the spectrum differing maximally by less than a percent at $p_t = 20$ GeV, at hadron level). See text for further details.

that there are other processes for which this would not be true, e.g. inclusive b -jet production [2], and a case-by-case study is needed to establish whether any-flavour and net-flavour recombination are similar for a given process.

C. Full flavour at parton level in $pp \rightarrow Z + j$

Our final hadron-collider test is carried out at parton level (after showering) and applies jet flavour algorithms to all flavours of partons in the context of events with a hard jet recoiling against a high- p_t Z boson. This study is not intended to be of direct experimental relevance, but rather to test the flavour algorithm’s performance and limitations for addressing more theoretical questions such as the fractions of quark v. gluon jets. In particular, knowledge of the quark v. gluon fractions in a given sample is important when assessing the performance of approaches that attempt to distinguish quark v. gluon-induced jets from jet substructure and energy flow observables [49]. To do so we study $pp \rightarrow Z + j$ events. We focus here on the $Z(\rightarrow \mu^+\mu^-) + q$ final state, where we require exactly two muons to reconstruct a high- p_t Z candidate:

$$|\eta_\mu| < 2.4, \quad p_{t\mu} > 20 \text{ GeV}, \quad (15a)$$

$$p_{t,\mu^+\mu^-} > 1 \text{ TeV}, \quad m_{\mu^+\mu^-} \in [80, 102] \text{ GeV}. \quad (15b)$$

We find qualitatively consistent results for the $Z + g$ case.

We use Pythia 8.306 with the Monash13 tune to generate the events, and specifically consider its $pp \rightarrow Z + q$ process. We cluster the events with a given jet algorithm, and examine the flavour of the leading- p_t jet. At leading order, we expect the hard recoiling jet to always carry the flavour of the underlying quark or antiquark, and the question that we examine is that of how often the leading jet in the full showered sample has a flavour other than that of a single quark or anti-quark.

Schematically, it is useful to think of two mechanisms that can cause the flavour to differ. One is that the quark can split to $q + g$ with a separation $\Delta R_{qg} > R$. If the gluon carries more energy than the quark, then the leading jet will actually be a gluon jet. The rate for this to happen is logarithmically enhanced in the small- R limit [50]. The second mechanism to keep in mind is the contamination of the flavour of a hard quark jet from a soft $g \rightarrow q\bar{q}$ splitting (i.e. the issue of Fig. 1, which flavoured jet algorithms are supposed to mitigate against). This can have two effects: if the soft $q\bar{q}$ pair’s flavour coincides with that of the jet, then it can cancel the jet’s flavour; much more often, a fraction $\sim 1 - 1/(2n_f)$ of the time, it will lead to a multi-flavour jet. To a first approximation, this effect is expected to grow with increasing jet radius. We show results both with and without multi-parton interactions (MPI), and

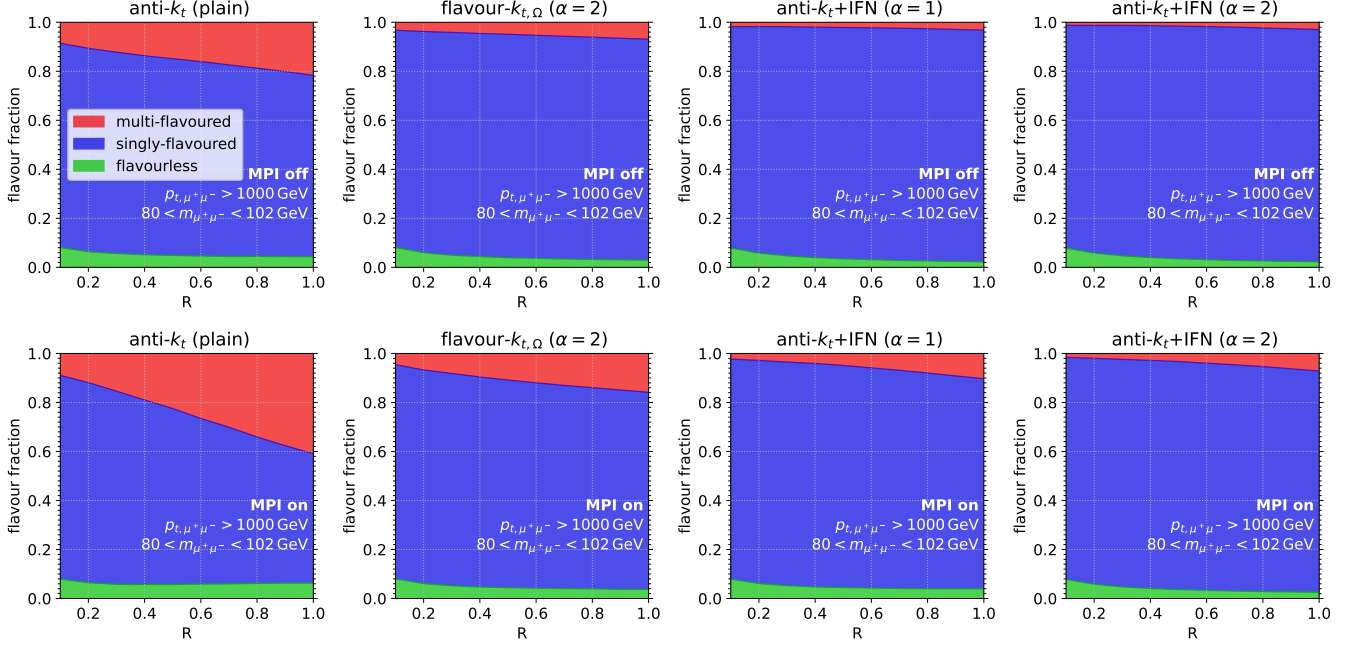


FIG. 10. Stress-tests of the performance of the plain anti- k_t algorithm (with net flavour summation, left column), the flavour- $k_{t,\Omega}$ algorithm (middle left column), and the anti- k_t algorithm with flavour neutralisation (with $\alpha = 1$, middle right column, and $\alpha = 2$, right column). The stress-tests are performed in $pp \rightarrow Z + q$ collisions with $p_{tZ} > 1$ TeV, as simulated with Pythia 8.3 at parton level with multi-parton interactions disabled (enabled) on the upper row (lower row). As a function of the jet radius parameter R , the plots show the fraction of leading jets that are multi-flavoured, i.e. whose flavour is neither that of a gluon nor a single quark or anti-quark (red band), singly flavoured (blue band) and flavourless (green band). The key observation is the large fraction of multi-flavoured jets with the standard anti- k_t algorithm, which occur due to contamination of the hard jet flavour from low-momentum particles. With the flavour- $k_{t,\Omega}$ algorithm, we see some reduction, while anti- k_t with IFN shows a further reduced rate, especially for $\alpha = 2$.

we expect the flavour contamination to be worsened by MPI, insofar as it adds significant numbers of additional low- p_t $q\bar{q}$ pairs.

In Fig. 10, we show the fraction of leading- p_t jets that are flavourless (green), singly-flavoured (quark or anti-quark, blue) or multi-flavoured (neither flavourless or singly-flavoured, red), as a function of the jet radius parameter R used in the clustering. We perform this comparison with Pythia at parton level, where the underlying event is turned off (upper row), and with MPI turned on (lower row). From left to right, the columns show results with the standard anti- k_t algorithm, flavour- $k_{t,\Omega}$ ($\alpha = 2$), and anti- k_t with our IFN algorithm for two values of $\alpha = \{1, 2\}$ (and $\omega = 3 - \alpha$). A first point to observe is the large multi-flavoured contribution for the plain anti- k_t algorithm, about 14% at $R = 0.4$ without MPI, increasing to 19% with MPI. Increasing R substantially worsens the situation with over 40% multi-flavoured jets for $R = 1$ when MPI is on.

Flavour- $k_{t,\Omega}$ improves the situation somewhat, giving a multi-flavoured contribution of 5% (10%) with MPI off (on) at $R = 0.4$. The anti- k_t algorithm with IFN brings a more substantial improvement, yielding 2% (4%) for

$\alpha = 1$ and 1.5% (3%) for $\alpha = 2$.¹⁶

Examining instead the unflavoured (“gluon”) jet fractions, we find that all flavour algorithms give a $\sim 4\%$ gluon-jet fraction at $R = 0.4$, relatively unaffected by the presence of MPI. This figure is important to keep in mind for quark/gluon discrimination studies [49]: the fact that a jet was initiated by a quark in Pythia does not mean that the corresponding jet observed after showering is always a quark jet. In particular, Fig. 10 implies that if one is attempting to tag gluon-jets and reject quark-jets, and one is using Pythia’s $Z + q$ and $Z + g$ samples as the sources of quark and gluon jets, then even a perfect gluon tagger will still show an acceptance of about 4% on the $Z + q$ sample.

Ultimately, we would argue that the “truth” flavour labels should be derived not from the generation process, but by running a jet flavour algorithm such as anti- k_t +IFN. Nevertheless the anti- k_t +IFN labelling remains subject to some ambiguities, and the multi-flavoured jet fraction discussed above is probably a good measure of

¹⁶ For the CMP_Ω algorithm there is freedom in how one extends it to multi-flavoured events, and accordingly we defer study of multi-flavoured events with that algorithm to future work.

those ambiguities. As a future direction, one might wish to investigate whether one can develop jet flavour algorithms that further reduce the multi-flavoured jet fraction, while maintaining other good properties.

VI. EXPLORATION OF IFN ALGORITHM FOR e^+e^- COLLISIONS

The IFN algorithm for e^+e^- collisions follows the same set of rules as the pp version in Sec. III, adapting the u_{ij} distances so that they coincide with the e^+e^- flavour- k_t distances, specifically

$$u_{ik} \equiv [\max(E_i, E_k)]^\alpha [\min(E_i, E_k)]^{2-\alpha} \times 2(1 - \cos \theta_{ik}). \quad (16)$$

In contrast with the hadron-collider case, there is no need to use a modified angular distance in the e^+e^- form of the u_{ij} . Additionally in step 1 of the part of the algorithm in Sec. IIIB, we define i to be the particle with lower energy.

We have not explicitly performed the same full set of IRC safety tests on the e^+e^- algorithm that we carried out in the pp case. The issues identified across various algorithms in the pp case fall into two classes: those involving initial-state hard-collinear radiation, which is irrelevant in the e^+e^- case, and those involving just the interplay between final-state soft large-angle and hard-collinear branchings. The analyses of these latter issues in App. C are expected to be insensitive to the differences between Eqs. (16) and (7). For this reason, we do not anticipate IRC safety issues in the e^+e^- , though a detailed study would ultimately be desirable.

The relatively clean environment of e^+e^- collisions allows for a further exploration of the performance of IFN-style algorithms. Specifically, we take a parton shower simulation of $e^+e^- \rightarrow q\bar{q}$ events, cluster each event into two jets, and examine the flavours of those two jets. Typically one expects each jet to have the flavour of the parton in the Born event. In analogy with our pp study of Fig. 10, we examine the fraction of events where this does not happen, breaking it into two components, one where each jet is flavourless (“gg”) and the other where the two jets have neither the original $q\bar{q}$ flavour nor gg flavour (“other”). We plot these fractions as a function of \sqrt{s} . For a well-behaved flavour algorithm, we expect the rate of gg configurations to decrease with increasing \sqrt{s} , as $\alpha_s(\sqrt{s})$, associated with the probability of producing a $q\bar{q}q$ configuration where the $q\bar{q}$ pair ends up back-to-back with respect to the gluon. Similarly, the rate of “other” configurations should decrease as $\alpha_s^2(\sqrt{s})$, since one expects to have to generate a hard $q\bar{q}q'\bar{q}'$ configuration to obtain an “other” flavour.

We carry out the parton shower simulation with Pythia 8.306 (4C tune) at parton level. The jet clustering is performed as follows: for the k_t and C/A algorithms, we use a large radius $R = 2\pi$ and then decluster the event back to two jets by undoing the last stage of the

clustering in order to obtain the two hard jets. This is equivalent to asking for two hard jets in the normal exclusive k_t or Cambridge algorithms. For the anti- k_t algorithm we use a jet radius of $R = 3\pi/4$ and take the two highest energy jets. The specific jet radius choice is designed to be large enough that events with multiple well separated hard partons still only give two hard jets, but small enough that opposite hemispheres of the event do not cluster together.

Fig. 11 shows the gg (left column) and “other” (right column) rates as a function of \sqrt{s} in the range 100 GeV to 10^5 GeV. This broad (and today unrealistic) energy range is intended to help visualise the scaling behaviour of the rates. Each row corresponds to one underlying jet algorithm, with different curves showing results for different flavour approaches. Let us start by examining the gg rate for the anti- k_t algorithm and its IFN variants (top-left panel). Over the energy range being considered, α_s decreases by almost a factor of two. The anti- k_t +IFN algorithms show a gg rate that is more or less consistent with $\alpha_s(\sqrt{s})$ scaling. In contrast the plain anti- k_t algorithm (with net flavour summation) features a rate that slowly increases. It is natural to ascribe the growth to the IRC unsafety of the algorithm, however the differences between the safe (IFN) and unsafe (plain anti- k_t) variants remain relatively modest.

The situation becomes clearer when looking at the “other” flavour combinations (top-right panel). Here the plain anti- k_t algorithm gives a rate that increases from about 10% at $\sqrt{s} = 100$ GeV to almost 30% at $\sqrt{s} = 10^5$ GeV. In contrast, the IRC-safe IFN variants give much smaller rates, well below 2% across the whole energy range, i.e. a huge improvement on the plain anti- k_t algorithm. With the $\alpha = 1$ IFN choice, the rate decreases more or less consistently with the expectation of α_s^2 scaling. The $\alpha = 2$ IFN algorithm shows a lower rate, but also a slower scaling. The situation is broadly similar for the C/A algorithm, with the IFN rate a little higher. For the k_t family, we show only the plain k_t algorithm and the flavour- k_t algorithm, since we have not conclusively validated the IRC safety of the k_t +IFN combination. Interestingly the flavour- k_t algorithm shows only modest improvement in the “other” rate relative to the plain k_t algorithm, and a scaling that is no better.

It is intriguing that different IRC safe algorithms lead to “other” rates that have varying degrees of consistency with the expected α_s^2 scaling. While we do not yet have a complete understanding of this phenomenon, detailed investigations into the events have revealed all-order mechanisms that operate across multiple scales and that, in some situations, cause soft flavour to be successively associated with harder and harder momenta, ultimately transferring soft flavour to the hard jets. Further study would require detailed analysis of the interplay between the main jet algorithm’s clustering sequence and the IFN flavour neutralisation scales. Still, despite these observations, the IFN algorithms clearly perform much better than plain flavour unsafe ones, indicating the substantial

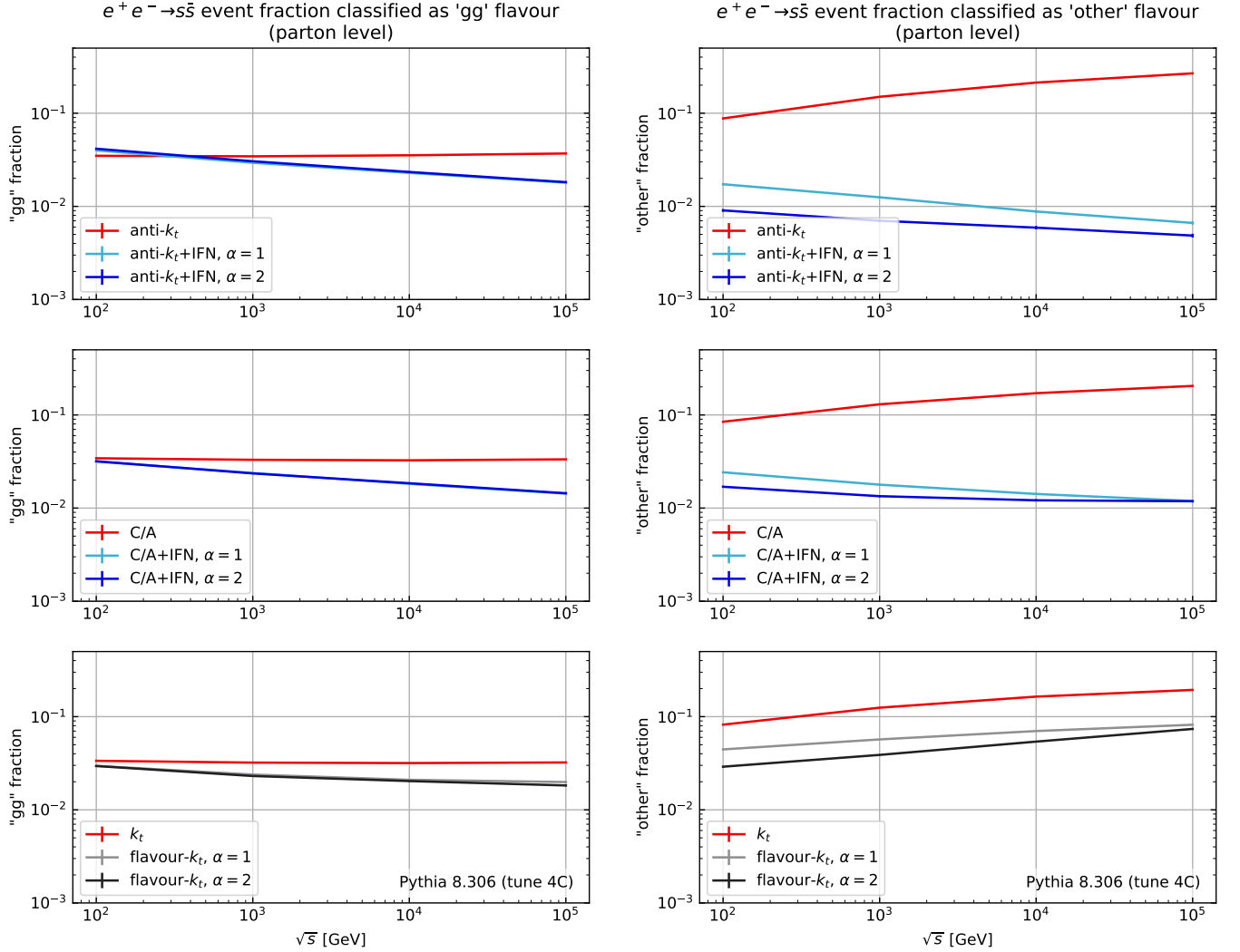


FIG. 11. The fraction of $e^+e^- \rightarrow q\bar{q}$ events (after parton showering and clustering to two jets), in which the flavour of the two jets is classified as being gg (left column) or any other combination that is not the original $q\bar{q}$ (right column). The results are shown as a function of \sqrt{s} for algorithms in the anti- k_t family (top row), the C/A family (middle row) and k_t family (lower row). The results have been obtained using Pythia 8.306 at parton level, with tune 4C.

benefits for detailed flavour studies in using a suitably chosen flavour-safe algorithm.

VII. CONCLUSIONS AND OUTLOOK

In this article, we introduced an approach to jet clustering that maintains the kinematics of the original anti- k_t and C/A algorithms, while also providing IRC-safe jet-flavour identification. Our IFN algorithm has passed a battery of fixed-order IRC safety tests, which revealed a number of unexpected and subtle issues in prior jet-flavour proposals. While not an absolute guarantee, these tests do provide a reasonable degree of confidence in the IRC safety of our approach. On three benchmark jet flavour tasks, IFN exhibits the desired phenomenological

behaviour. These studies suggest that IFN can yield a theoretically sound meaning to the concept of a flavoured jet in the majority of heavy-flavour related applications that can be envisaged at the LHC.

There are various experimental considerations that should be noted before deploying IFN in a full analysis. Our algorithm, like all other attempts at IRC-safe flavour jet algorithms, requires the complete flavour information in the event for those flavours under consideration, e.g. b -flavour. This is highly challenging in an experimental environment, because of the difficulties of tagging low-momentum single B -hadrons, as well as quasi-collinear pairs of B -hadrons. The question remains, however, whether recent advances in machine-learning can help reveal the information that is needed, and more generally whether experimentally one can unfold detector-

level results to particle-level jet definitions such as ours. Furthermore, for certain signal processes, the practical impact of this issue may only be moderate, cf. the $\lesssim 3\%$ difference between the any-flavour and net-flavour anti- k_t results for $t\bar{t}$ (Fig. 9 right).

Theoretically, we stress that the concept of jet flavour remains subtle also beyond the scope of the discussion in this article. We focused on the fixed-order behaviour, but there can be non-trivial interplay with the still perturbative but complex structure induced by all-order showered events. Beyond a perturbative analysis, there are even more difficult issues of jet flavour in the presence of the high densities of flavoured particles that result from hadronisation. These questions warrant more investigation. Nevertheless, the IFN algorithm developed here already shows clear and substantial benefits both with respect to standard unflavoured algorithms and to prior incarnations of flavoured algorithms.

Code implementing the IFN algorithm is available from <https://github.com/jetflav/IFNPlugin>, in the form of a FastJet Plugin.

ACKNOWLEDGEMENTS

We are grateful to Andrea Banfi, Simone Marzani and Giulia Zanderighi for helpful discussions and comments on the manuscript. We are also grateful to the authors of Refs. [10] and [11] for discussions about their respective algorithms and more generally on these topics. GPS and LS would also like to thank their PanScales collaborators for joint work on the high-precision adaptations of the `fjcore` code used in the IRC safety tests. GPS would also like to thank Matteo Cacciari and Gregory Soyez for joint work on updates to FastJet to facilitate the inclusion of flavour in plugins.

This work has been funded by a Royal Society Research Professorship (RP\R1\180112) (GPS+LS), by the European Research Council (ERC) under the European Union's Horizon 2020 research and innovation programme (grant agreement No. 788223, PanScales, GPS+LS+MH; and grant agreement 804394, HipQCD, FC) and by the Science and Technology Facilities Council (STFC) under grants ST/T000864/1 and by Somerville College (LS). JT is supported by the U.S. DOE Office of High Energy Physics under Grant Contract No. DE-SC0012567. RG is supported by the STFC, a Wolfson Harrison UK Research Council Physics Scholarship and by a Clarendon Scholarship, and in the early stages of this work benefited from support from Merton College. Part of this work benefited from the support and hospitality of the Munich Institute for Astro-, Particle and BioPhysics (MIAPbP) which is funded by the Deutsche Forschungsgemeinschaft (DFG, German Research Foundation) under Germany's Excellence Strategy – EXC-2094 – 390783311.

Appendix A: Asymmetric double-soft branching

As discussed in Fig. 1, the classic IRC safety issue involves configurations with a double-soft $g \rightarrow q\bar{q}$ pair. One surprising feature that we will encounter in Apps. B 1, C 1 and C 3 is that the structure of higher-order IRC divergences in some algorithms is sensitive to configurations where one of the quarks is significantly softer than the other. Consequently, it is important to understand the asymptotic behaviour of double soft $q\bar{q}$ production in such limits.

We know that collinear $g \rightarrow q\bar{q}$ splitting comes with a $P_{qg}(z)dz = T_R(z^2 + (1-z)^2)dz$ structure, which is finite and non-zero when $z \rightarrow 0$. One question one might ask, though, is whether the splitting probability remains finite and non-zero for $z \rightarrow 0$ when the pair is not collinear but instead separated by an angle that is commensurate with the emission angle of the parent gluon. In this appendix, we find that the splitting probability is indeed finite in that limit, and we derive a simple approximate expression for its behaviour.

Consider a process with n hard massless QCD partons with momenta $\{p_i\}$ and study the emission of two additional soft quarks with momenta $q_{1,2}$. The double-soft emission probability can be written as a sum over dipole contributions as

$$d\mathcal{P}_{\text{d.s.}} = - \sum_{i \neq j=1}^n \mathbf{T}_i \cdot \mathbf{T}_j d\mathcal{P}_{\text{d.s.}}^{(i,j)}, \quad (\text{A1})$$

where \mathbf{T}_i are the standard colour operators (see e.g. Ref. [51] for details) and $d\mathcal{P}^{(i,j)}$ only depends on the momenta of the soft quarks and of the hard partons i and j . To write an explicit representation for $d\mathcal{P}^{(i,j)}$, it is convenient to work in the dipole centre-of-mass frame. Specifically, we write

$$\begin{aligned} p_i &= E(1; 0, 0, 1), \\ p_j &= E(1; 0, 0, -1), \\ q_1 &= p_{t,1}(\cosh y_1; 1, 0, \sinh y_1), \\ q_2 &= p_{t,2}(\cosh y_2; \cos \Delta\phi, \sin \Delta\phi, \sinh y_2). \end{aligned} \quad (\text{A2})$$

We stress that $p_{t,1,2}$, $y_{1,2}$ and $\Delta\phi$ are dipole-specific and not global variables. In terms of these variables, the double-soft emission probability reads

$$\begin{aligned} d\mathcal{P}_{\text{d.s.}}^{(i,j)} &= \left(\frac{\alpha_s}{2\pi}\right)^2 4T_R dp_{t,1} dp_{t,2} dy_1 d\Delta y \frac{d\Delta\phi}{2\pi} \times \\ &\frac{2p_{t,1}p_{t,2} - (p_{t,1}^2 + p_{t,2}^2) \cos \Delta\phi + |\vec{p}_{t,1} - \vec{p}_{t,2}|^2 \cosh \Delta y}{(p_{t,1}^2 + p_{t,2}^2 + 2p_{t,1}p_{t,2} \cosh \Delta y)^2 (\cosh \Delta y - \cos \Delta\phi)^2}, \end{aligned} \quad (\text{A3})$$

where $\Delta y = y_2 - y_1$ and $T_R = 1/2$. In the limit when the soft quark pair is also collinear to parton i , Eq. (A1) simplifies to

$$d\mathcal{P}_{\text{d.s.}} = - \sum_{i \neq j=1}^n \mathbf{T}_i \cdot \mathbf{T}_j d\mathcal{P}_{\text{d.s.}}^{(i,j)} \rightarrow C_i d\mathcal{P}_{\text{d.s.}}^{(i,j)}, \quad (\text{A4})$$

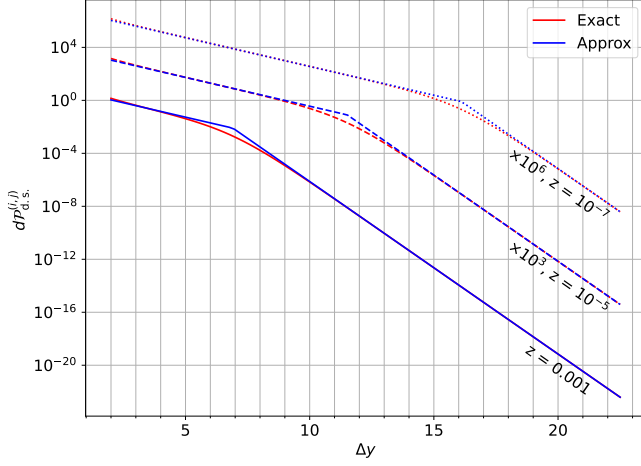


FIG. 12. The double-soft matrix element $d\mathcal{P}_{\text{d.s.}}^{(i,j)}$ in (red) its exact form from Eq. (A3), and in (blue) the approximate form from Eq. (A8) that we use in our numerical IRC-safety tests, as a function of the rapidity separation Δy of the two soft partons in the dipole centre-of-mass frame. The matrix element is plotted for $p_{t,1} = 1$ GeV, and $\Delta\phi = 0$, for several values of z (shown as full, dashed and dotted lines). The two regimes with $\sim e^{-\Delta y}$ and $\sim e^{-3\Delta y}$ scaling are clearly visible.

with $d\mathcal{P}_{\text{d.s.}}^{(i,j)}$ still given by Eq. (A3) and where $C_i = C_A$ if parton i is a gluon and $C_i = C_F$ if it is a quark.

We can now study the asymmetric $p_{t,2} \ll p_{t,1}$ configuration. We write $p_{t,2} = zp_{t,1}$. In the small- z region, Eq. (A3) becomes

$$d\mathcal{P}_{\text{d.s.}}^{(i,j)} \sim \left(\frac{\alpha_s}{2\pi}\right)^2 \frac{4T_R dp_{t,1} dz dy_1 d\Delta y d\Delta\phi}{2\pi p_{t,1} (\cosh \Delta y - \cos \Delta\phi)}. \quad (\text{A5})$$

We see that, as for the P_{qg} splitting function, this probability is finite and non-zero for $z \rightarrow 0$. For our analysis, we also find it useful to consider Eq. (A3) in the limit of large rapidity separation between the two soft quarks, $\Delta y \gg 1$. We obtain

$$d\mathcal{P}_{\text{d.s.}}^{(i,j)} \sim \left(\frac{\alpha_s}{2\pi}\right)^2 8T_R \frac{dp_{t,1}}{p_{t,1}} \frac{dp_{t,2}}{p_{t,2}} dy_1 d\Delta y \frac{d\Delta\phi}{2\pi} \times \frac{p_{t,1} p_{t,2} e^{-\Delta y}}{(p_{t,1} + e^{\Delta y} p_{t,2})^2}. \quad (\text{A6})$$

In the asymptotic regime, the second line of Eq. (A6) is well approximated by the following expression

$$\frac{p_{t,1} p_{t,2} e^{-\Delta y}}{(p_{t,1} + e^{\Delta y} p_{t,2})^2} \approx \min \left[\frac{p_{t,1}}{p_{t,2}} e^{-3\Delta y}, \frac{p_{t,2}}{p_{t,1}} e^{-\Delta y} \right], \quad (\text{A7})$$

which interpolates between the $1 \ll \ln(p_{t,1}/p_{t,2}) \ll \Delta y$ and $1 \ll \Delta y \ll \ln(p_{t,1}/p_{t,2})$ limits.

In practice, we find that this interpolation works well across the whole phase space. As shown in Fig. 12, we

find that

$$d\mathcal{P}_{\text{d.s.,approx}}^{(i,j)} \equiv \left(\frac{\alpha_s}{2\pi}\right)^2 8T_R \frac{dp_{t,1}}{p_{t,1}} \frac{dp_{t,2}}{p_{t,2}} dy_1 d\Delta y \frac{d\Delta\phi}{2\pi} \times \min \left[\frac{p_{t,1}}{p_{t,2}} e^{-3\Delta y}, \frac{p_{t,2}}{p_{t,1}} e^{-\Delta y} \right] \quad (\text{A8})$$

provides a good approximation of the exact $d\mathcal{P}_{\text{d.s.}}^{(i,j)}$ result down to values of $\ln(p_{t,1}/p_{t,2})$ and Δy of order 1. Furthermore, it is free of the collinear divergence when the q and \bar{q} go close in angle, a collinear divergence that we deliberately wish to leave out, because of our approach of allowing at most one divergence (or logarithm) per power of α_s . In our studies, we therefore use the convenient interpolation Eq. (A8) rather than the exact result Eq. (A3).

Appendix B: Numerical tests of IFN

In the process of developing the IFN algorithm, we tested a number of possible variants. In this appendix, we provide numerical support for the analytic arguments made in Sec. III to justify our design choices.

1. Relation between α and ω

According to the arguments in Sec. III C, we need to take particular care in choosing the values of the parameters α and ω in the IFN algorithms. A potentially dangerous configuration is that presented in Fig. 3. In that diagram, two partons (one flavoured, one flavourless) at central rapidity are clustered together by the anti- k_t algorithm. In our IFN algorithms, the IRC safety issue arises from an initial-state hard-collinear splitting, which can act as a possible neutralisation partner for the flavoured “hard” particle. As argued in Eq. (9), the condition $\alpha + \omega > 2$ ensures that such a neutralisation does not happen.

To test this argument numerically, we integrate uniformly over the momentum of each of a central hard quark and hard gluon (each in the range 1 GeV to 1 TeV) and sample an IHC emission as described in Sec. IV A. The results are presented in Fig. 13, for various values of the parameters α and ω . As expected, in cases where $\alpha + \omega < 2$, as well as for IFN variants that use a ΔR_{ij}^2 type angular distance instead of our Ω_{ij}^2 , the failure rate typically diverges for $p_{t,\text{max}} \rightarrow 0$, and conversely falls off as a power law when $\alpha + \omega > 2$ (green and blue curves). We observe numerically that the border cases, $\alpha + \omega = 2$, are all unsafe.

Let us see analytically why $\alpha + \omega = 2$ is problematic for the specific case of $\alpha = 2$ (and $\omega = 0$). We note that in the limit where $\omega \rightarrow 0$, the angular factor Ω_{ik}^2 in Eq. (7b) differs from ΔR_{ik}^2 at most by a factor of $\mathcal{O}(1)$, which we can typically neglect in the discussions below. We take the configuration shown in Fig. 3 with $p_{t2} = z_2 p_{t3}$ with

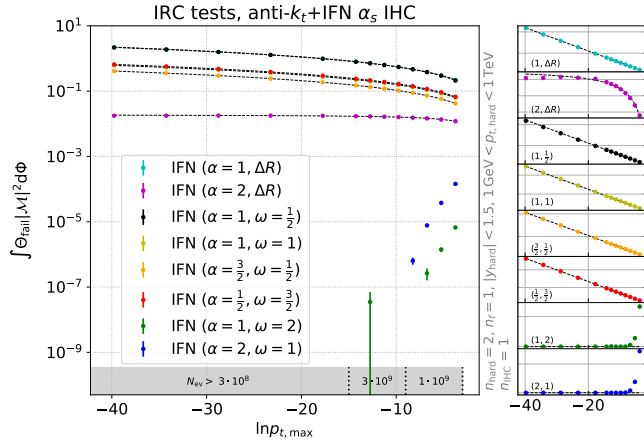


FIG. 13. IRC safety tests of anti- k_t +IFN for variants with different angular scaling factors. The tested configuration from Fig. 3 features two hard partons clustered together by the anti- k_t algorithm and one initial-state hard-collinear splitting. With a ΔR_{ij}^2 angular factor, the IFN algorithms diverge for all choices of α . Switching to the Ω_{ij}^2 angular distance, the cases where $\alpha + \omega \leq 2$ also diverge, whereas for $\alpha + \omega > 2$, they converge to zero as a power law, as expected from Eq. (9). The right-hand side-panels show the results on a linear scale, to help visualise the scaling for the IRC-unsafe variants. Note that here and in some of the following figures, certain curves differ in the number of generated events. Because the multiple curves feature different scaling behaviours, they require a varying number of events to make a conclusive statement about the form of the divergence (or the absence thereof). The smallest number of events generated among all runs performed for a given figure is shown in the three shaded regions at the bottom of the plot.

$z_2 \ll 1$, $p_{t3} = 1$. There are two competing distances in the neutralisation step,

$$u_{12} = z_2^2 \Delta y_{12}^2 \simeq z_2^2 \ln^2 1/p_{t1}, \quad (\text{B1a})$$

$$u_{23} = \Delta R_{23}^2 \sim 1. \quad (\text{B1b})$$

The IFN algorithm will neutralise the flavours of 1 and 2 when $z_2 \ln 1/p_{t1} < \Delta R_{23}$. If we integrate over the momentum of 2 and assume a dz_2 distribution (see e.g. [52]) for finite ΔR_{23} and take $z_2 \rightarrow 0$, then the resulting integral is given by $\int d \ln p_{t1} \int_0^{1/\ln p_{t1}} dz_2$, which diverges. The analytic argument shown here does not apply to generic values of α and ω , but as mentioned above, we find numerically that all cases that we have tested with $\alpha + \omega = 2$ diverge.

2. Recursive v. non-recursive

In Sec. IIID, we presented an analytic argument to explain why the IFN algorithms need a recursion step. Fig. 14 shows the failure rate events with two hard partons and one IDS pair, which includes configurations such as that of Fig. 4. It clearly shows that without recursion,

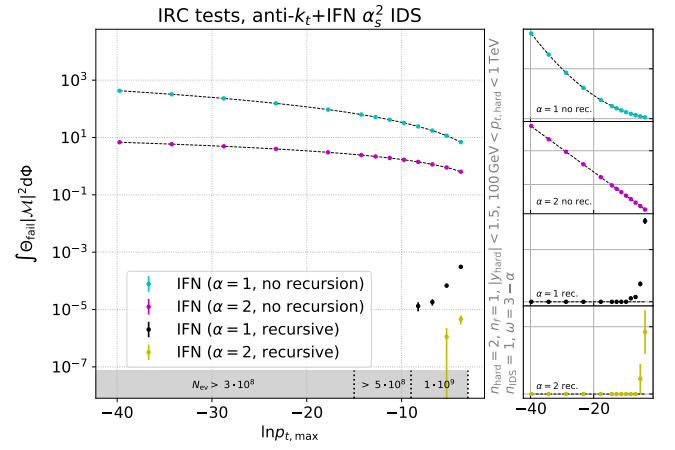


FIG. 14. IRC safety test of anti- k_t +IFN for variants with and without the recursion step. The tested events consist of two hard partons supplemented with one initial-state double soft pair, as in Fig. 4.

the algorithm shows a growing failure rate for $p_{t,max} \rightarrow 0$, while the failure vanishes for $p_{t,max} \rightarrow 0$ with the recursive step turned on. The side-figures help illustrate that the failure rate goes as $\ln^2 p_{t,max}$ for $\alpha = 1$ and as $\ln p_{t,max}$ for $\alpha = 2$. The stronger power for $\alpha = 1$ arises because failures can happen even when the IDS pair is collinear to the beams.

Appendix C: IRC-unsafe configurations

In this appendix, we analyse the specific IRC-unsafe configurations identified in Sec. IVD for the flavour- k_t , CMP and GHS algorithms. For each of the configurations that we have identified, we present both analytic and numerical results to demonstrate why they are problematic. Throughout this section we define $p_{ti} \lesssim p_{tj}$ to mean that $p_{ti} < p_{tj}$ but that they are of similar orders of magnitude.

1. IHC×IDS subtlety at α_s^3 for flavour- k_t

The flavour- k_t (and GHS) algorithms encounter a problematic configuration at order α_s^3 , shown in Fig. 15, associated with the choice of angular measure. There is a hard parton (1, with flavour q) that produces the only hard jet in the event, together with a soft gluon g that splits to a soft large-angle $q\bar{q}$ pair (2 and 3), and additionally an initial-state collinear gluon splitting that produces an energetic small-angle quark of flavour \bar{q} (4). For the sake of the discussion, we assume that the transverse momentum of 2 is smaller than that of 3, by a factor z_{23} ,

$$p_{t2} = z_{23} p_{t3}. \quad (\text{C1})$$

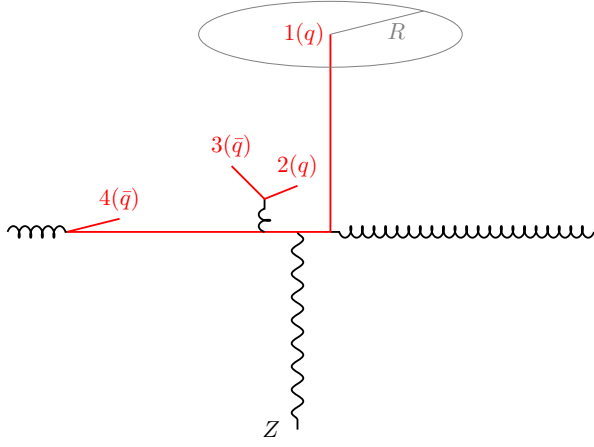


FIG. 15. Example configuration to illustrate issues that arise across multiple algorithms when using a standard ΔR type angular measure in inter-particle distances.

We take the rapidity and azimuth of 1 to be zero, $y_1 = \phi_1 = 0$. Additionally, we take $E_4 = z_{41}E_1$, which implies

$$y_4 = \ln \frac{2z_{41}p_{t1}}{p_{t4}}. \quad (C2)$$

For concreteness, we work with the $\alpha = 2$, $R = 1$ variant of the flavour- k_t algorithm. The inter-particle distances for the flavour- k_t algorithm were given in Eq. (2), and additionally we will need to take into account a beam distance with the right-moving beam. When i is flavoured (as it will always be in the example here),

$$d_{iB}^{\text{flav-}k_t} = [\max(p_{ti}, p_{tB}(y_i))]^\alpha [\min(p_{ti}, p_{tB}(y_i))]^{2-\alpha}, \quad (C3)$$

with

$$p_{tB}(y) = \sum_i p_{ti} [\Theta(y - y_i)e^{y_i - y} + \Theta(y_i - y)], \quad (C4)$$

so that

$$p_{tB}(0) \simeq p_{t1}, \quad (C5a)$$

$$p_{tB}(y_4) \simeq p_{t4} + p_{t1}e^{-y_4} \simeq p_{t4} \left(1 + \frac{1}{2z_{41}}\right), \quad (C5b)$$

where we have used the fact that $p_{t4} \ll p_{t1}$. In the absence of the soft quark pair, there are three distances,

$$d_{14} = p_{t1}^2 \Delta R_{14}^2 \simeq p_{t1}^2 y_4^2, \quad (C6a)$$

$$d_{1B} \simeq p_{t1}^2, \quad (C6b)$$

$$d_{4B} \simeq p_{t4}^2 \left(1 + \frac{1}{2z_{41}}\right)^2. \quad (C6c)$$

The smallest is d_{4B} , since $p_{t4}/z_{41} \ll p_{t1}$ and so initial-state collinear particle 4 clusters first, leaving a flavoured jet consisting of particle 1.

Now we examine the additional distances that arise when the soft $q\bar{q}$ (23) pair is present. The beam distances

d_{2B} and d_{3B} are both similar to $d_{1B} = p_{t1}^2$, since they are at central rapidities where $p_{tB} \sim p_{t1}$. The distances that will matter for the clustering are

$$d_{23} = p_{t3}^2 \Delta R_{23}^2 \sim \frac{p_{t2}^2}{z_{23}^2}, \quad (C7a)$$

$$d_{24} = \max(p_{t4}^2, p_{t2}^2) \Delta R_{24}^2 \sim \max(p_{t4}^2, p_{t2}^2) \ln^2 \frac{z_{41}^2 p_{t1}^2}{p_{t4}^2}, \quad (C7b)$$

where \sim implies that we leave out factors of $\mathcal{O}(1)$, e.g. from $\Delta R_{23}^2 \sim 1$. We neglect d_{34} , since in the moderately small z_{23} limit where we will be working (cf. Eq. (C1)), $d_{34} > d_{24}$.

If d_{23} is the smallest of the distances across Eqs. (C6) and (C7), particles 2 and 3 annihilate, then 4 clusters with the beam, and the hard jet has flavour q . If d_{4B} is the smallest, 4 clusters with the beam, then 2 and 3 annihilate and the hard jet has flavour q . The problematic situation is when d_{24} is the smallest of the distances, causing 2 and 4 to annihilate. This leaves 3, which can cluster with 1, resulting in a flavourless hard jet.

To understand the likelihood of this occurring, we first introduce the shorthand

$$\ell_{ij} = \ln \frac{p_{ti}}{p_{tj}}. \quad (C8)$$

Let us first consider $p_{t4} < p_{t2}$ ($\ell_{24} > 0$). The d_{24} will be the smallest one when

$$d_{24} < d_{23} \rightarrow \ell_{14} + \mathcal{O}(\ln z_{41}) < \frac{1}{z_{23}}, \quad (C9a)$$

$$d_{24} < d_{4B} \rightarrow \ell_{14} + \mathcal{O}(\ln z_{41}) < \frac{e^{-\ell_{24}}}{z_{41}}. \quad (C9b)$$

Ignoring azimuthal integrals (and the rapidity of 2 and 3), we now have to integrate over four phase-space variables, which we take to be ℓ_{14} , ℓ_{24} , z_{23} and z_{41} . We have found that we can ignore the $\mathcal{O}(\ln z_{41})$ terms in Eq. (C9) and rewrite the limits as

$$z_{23} < \frac{1}{\ell_{14}}, \quad z_{41} < \frac{e^{-\ell_{24}}}{\ell_{14}}, \quad [\ell_{24} > 0]. \quad (C10)$$

Since both z fractions will be small, we will perform the integrations over z_{23} and z_{41} using the constant small- z limit of $P_{g \rightarrow q\bar{q}}(z)dz$. The overall rate of 24 clustering (with $\ell_{24} > 0$) is then given by

$$N_{24, \text{flav-}k_t}^{(\ell_{24} > 0)} \sim \alpha_s^3 \int_0^\infty d\ell_{14} \int_0^{\ell_{14}} d\ell_{24} \int_0^{\frac{1}{\ell_{14}}} dz_{23} \int_0^{\frac{e^{-\ell_{24}}}{\ell_{14}}} dz_{41} \sim \alpha_s^3 \int_0^\infty \frac{d\ell_{14}}{\ell_{14}^2}, \quad (C11)$$

where in setting the lower limits of the ℓ_{14} and ℓ_{24} integrals to zero, we are ignoring any constraints from the interplay, e.g., with the z_{23} integral. A similar analysis

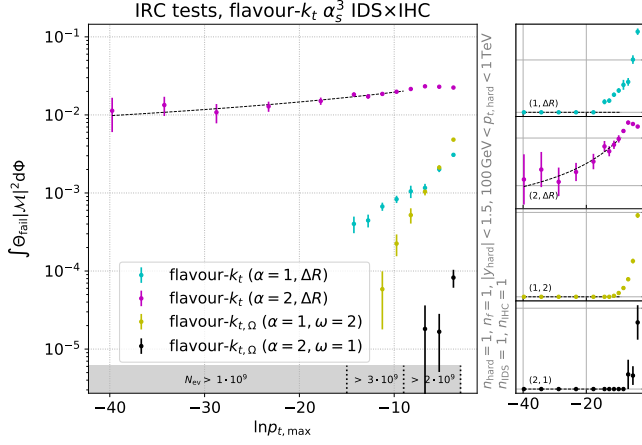


FIG. 16. Failure rate of the flavour- k_t algorithm for the configuration of Fig. 15, in particular illustrating results for $\alpha = 2$ (magenta points) that are qualitatively consistent with the expected $1/\ln p_{t,max}$ behaviour (dashed line). Also shown are results for $\alpha = 1$, as well as the results for flavour- $k_{t,\Omega}$, i.e. the adaptation with an Ω_{ij} angular distance, illustrating the much faster drop of the failure rate.

can be carried out for $\ell_{24} < 0$ (or equivalently $\ell_{42} > 0$), giving

$$z_{41} < \frac{1}{\ell_{14}}, \quad z_{23} < \frac{e^{-\ell_{42}}}{\ell_{14}}, \quad [\ell_{42} > 0], \quad (C12)$$

and yielding

$$N_{24, \text{flav-}k_t}^{(\ell_{42} > 0)} \sim \alpha_s^3 \int_0^\infty \frac{d\ell_{14}}{\ell_{14}^2}. \quad (C13)$$

This and Eq. (C11) both converge in the infrared, i.e. for $\ell_{14} \rightarrow \infty$, however this convergence is extremely slow. In particular, if one places an upper limit $p_{t4} > \epsilon$, the result converges as $(\ln 1/\epsilon)^{-1}$, which is consistent also with what we find in our numerical tests, cf. the magenta ($\alpha = 2$) points in Fig. 16. While this is strictly IRC safe at this order, one should worry that at the next order there may be logarithmic enhancements proportional to ℓ_{14} (for example from running-coupling effects), which would be sufficient to make the integral diverge. Accordingly, it would seem wise for future uses of the flavour- k_t algorithm to adopt the same kind of $\Delta R_{ij}^2 \rightarrow \Omega_{ij}^2$ replacement as used in our IFN algorithm, and similarly for any other algorithms that make use of similarly defined distances, e.g. the GHS flavour-dressing algorithm.

A final comment concerns the $\alpha = 1$ case. The analysis is somewhat more involved than for $\alpha = 2$, and it is also clear from Fig. 16 that the issue is reduced with $\alpha = 1$. Our investigations are consistent with a $1/\ln^p \epsilon$ scaling, with a larger value of p than for the $\alpha = 2$ case. One might wish to investigate this point further, however it would anyway seem wise to use the $\Delta R_{ij}^2 \rightarrow \Omega_{ij}^2$ replacement also for $\alpha = 1$.

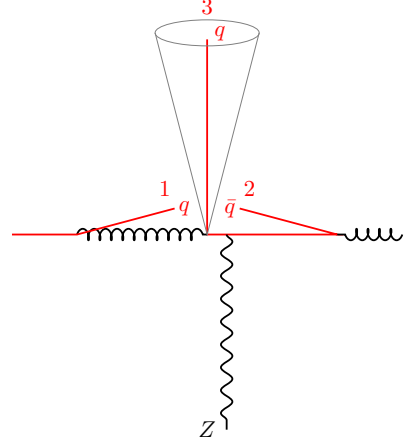


FIG. 17. Example $\mathcal{O}(\alpha_s^2)$ configuration that yields an issue for the CMP algorithm. There are two oppositely-flavoured initial-state hard-collinear splittings (b and \bar{b} , labelled 1 and 2), and a hard particle 3 at central rapidity.

2. IHC² issue at α_s^2 for CMP

An issue arises in the CMP algorithm at order α_s^2 for a configuration like the one shown in Fig. 17. We consider two initial-state hard-collinear emissions, a q and a \bar{q} (labelled 1 and 2), from the forward and backward beams respectively, and additionally one hard large-angle particle (numbered 3 in the figure). The initial-state hard-collinear emissions have a very small transverse momentum ($p_{t1}, p_{t2} \ll p_{t3}$) but large energies ($E_1, E_2 \sim E_3$). Let us assume $p_{t3} = E_3 = 1$, and particle 3 is simply aligned along the x -axis. Then we have that $y_1 \sim -\ln p_{t1}$ and $y_2 \sim \ln p_{t2}$ in the hard-collinear limit. For simplicity, we will work with $R = 1$.

The CMP algorithm will strongly favour clustering 1 and 2 together first. The global scale ($p_{t, \text{global-max}}$ in Eq. (5)) is set by the p_t of the hardest pseudojet currently available, p_{t3} , so the value of κ_{12} is small,

$$\kappa_{12} = \frac{1}{2a} \frac{p_{t1}^2 + p_{t2}^2}{p_{t3}^2} \ll 1, \quad (C14)$$

and the distance between the oppositely-flavoured particles 1 and 2 is thus given by

$$d_{12} = \frac{1}{\max(p_{t1}^2, p_{t2}^2)} \Delta R_{12}^2 \left(1 - \cos \left(\frac{\pi}{2} \kappa_{12} \right) \right) \quad (C15a)$$

$$\simeq \frac{1}{\max(p_{t1}^2, p_{t2}^2)} \Delta R_{12}^2 \frac{1}{2} \left(\frac{\pi}{2} \kappa_{12} \right)^2 \quad (C15b)$$

$$\simeq \frac{\pi^2}{32a^2} \Delta R_{12}^2 \frac{\max(p_{t1}^2, p_{t2}^2)}{p_{t3}^4}, \quad (C15c)$$

$$\simeq \frac{\pi^2}{32a^2} \left(\ln \frac{p_{t3}}{p_{t1}} + \ln \frac{p_{t3}}{p_{t2}} \right)^2 \frac{\max(p_{t1}^2, p_{t2}^2)}{p_{t3}^4}, \quad (C15d)$$

where ΔR_{12} is dominated by the large rapidity difference.

The other distances are

$$d_{iB} = \frac{1}{p_{ti}^2}, \quad i = \{1, 2, 3\}, \quad (\text{C16a})$$

$$d_{i3} \sim \frac{y_i^2}{p_{t3}^2}, \quad i = \{1, 2\}. \quad (\text{C16b})$$

When $p_{t1}, p_{t2} \ll p_{t3}$, it is straightforward to see that $d_{12} < d_{1B}, d_{2B}$ and $d_{12} < d_{13}, d_{23}$ (the logarithms in Eq. (C15d) have no impact on this). Therefore the first step of the algorithm will be to cluster particles 1 and 2, giving a flavourless pseudojet with transverse momentum, rapidity and squared invariant mass of

$$p_{t,(1+2)} \sim \max(p_{t1}, p_{t2}), \quad (\text{C17a})$$

$$y_{(1+2)} \simeq \frac{1}{2} \ln \frac{E_1}{E_2}, \quad (\text{C17b})$$

$$m_{(1+2)}^2 \simeq 4E_1 E_2. \quad (\text{C17c})$$

From the point of view of standard jet clustering, the $(1+2)$ pseudojet is unusual, because its transverse momentum is much smaller than its invariant mass.

The $(1+2)$ pseudojet will cluster with particle 3 if it is within a distance $\Delta R_{(1+2),3} < R = 1$. For any $p_{t1}, p_{t2} \ll p_{t3}$, there is always a finite azimuthal and E_1, E_2 phase space region such that that condition is satisfied, and the resulting $1+2+3$ cluster will have significantly different kinematics than particle 3, because of the extra energy brought by particles 1 and 2. Thus the jets can differ between the $1, 2, 3$ event and the event with just particle 3. The rate for this to happen is given by constants from the azimuthal and energy integrations multiplying divergent integrals over p_{t1} and p_{t2} ,

$$N \sim \alpha_s^2 \int_{\epsilon}^{p_{t3}} \frac{dp_{t1}}{p_{t1}} \int_{\epsilon}^{p_{t3}} \frac{dp_{t2}}{p_{t2}} = \alpha_s^2 \ln^2 \epsilon, \quad (\text{C18})$$

where we have explicitly included a cutoff scale ϵ in order to make the nature of the divergence manifest.

In Sec. IV D, we proposed a modification of the CMP algorithm, Eq. (11). For a generic ω , Eq. (C15d) in particular is replaced by

$$d_{12}^{(\Omega)} \sim \left(\frac{p_{t3}^2}{p_{t1} p_{t2}} \right)^{\omega} \frac{\max(p_{t1}^2, p_{t2}^2)}{p_{t3}^4}, \quad (\text{C19a})$$

$$\sim \frac{\max(p_{t1}^2, p_{t2}^2)}{p_{t1} p_{t2} p_{t3}^2} \cdot \left(\frac{p_{t3}^2}{p_{t1} p_{t2}} \right)^{\omega-1}. \quad (\text{C19b})$$

When $\omega = 1$, $d_{12}^{(\Omega)}$ will be of same order as d_{3B} if $p_{t1} \sim p_{t2}$. Schematically that suggests that there can still be a divergence of the form

$$N \sim \alpha_s^2 \int_{\epsilon}^{p_{t3}} \frac{dp_{t1}}{p_{t1}} \int_{\epsilon}^{p_{t3}} \frac{dp_{t2}}{p_{t2}} \delta(\ln p_{t2} - \ln p_{t1}) = \alpha_s^2 \ln \epsilon, \quad (\text{C20})$$

i.e. with one power of the logarithm. With a more complete calculation one can verify that that divergence is indeed present for $\omega = 1$. For $\omega > 1$, the second factor in

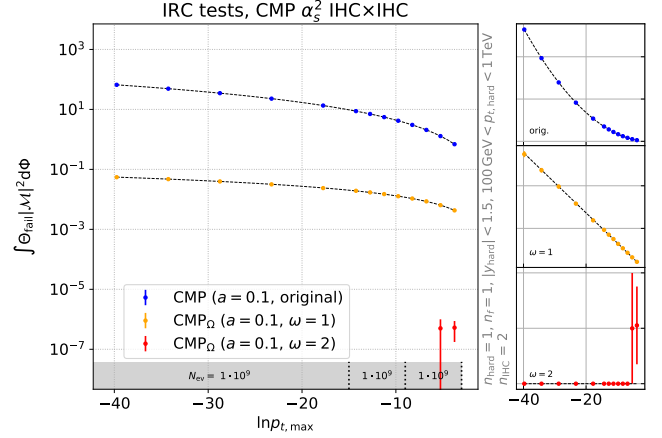


FIG. 18. Results of the numerical tests for CMP for a configuration as in Fig. 17, with the ΔR^2 angular factor in the distance measure, as in the original algorithm (in blue), and with a corrected angular factor as in Eq. (11) where $\omega = 1$ (in orange), and $\omega = 2$ (in red). Miniature plots on the right depict the integrated failure rate on a linear scale to help read the functional form of the divergence. The original algorithm suffers from a quadratic divergence, the corrected measure with $\omega = 1$ from a linear divergence, and the fix with $\omega = 2$ is IRC safe.

Eq. (C19b) instead ensures that $d_{12}^{(\Omega)} \gg d_{3B}$, thus ensuring particle 3 becomes a jet before any $1+2$ clustering, and resolving the IRC safety issue with the kinematics of jet 3.¹⁷

Results of the numerical IRC safety tests are presented in Fig. 18 for the original algorithm (with an angular factor ΔR^2 in the distance measure, in blue) and for the algorithm with an IRC-safe angular distance (for values of the parameter $\omega = 1$, in orange, and $\omega = 2$, in red). The results confirm the above analyses, showing a quadratic divergence in the original algorithm, while the divergence is linear for $\omega = 1$ and fully lifted for $\omega = 2$.¹⁸

¹⁷ Once particle 3 has been declared a jet and removed from the clustering, the $1+2$ cluster, if formed, would become a jet in its own right. Standard jet analyses place a cut on the jet p_t , which ensures that a residual lone massive, but low- p_t $1+2$ cluster does not count as a hard jet. However, one could imagine a scenario where one cuts not on p_t , but on $p_t^2 + m^2$, and in this case the $1+2$ cluster would count as an additional hard jet. In such a case, one could envisage that this would cause IRC unsafety even for $\omega > 1$. We have not explored this question further, insofar as analyses do not normally cut on $p_t^2 + m^2$.

¹⁸ Note that Fig. 1 (left) of Ref. [10] has studied $pp \rightarrow \ell^+ \ell^- b \bar{b}$ (with massless b 's), which should include the configuration of our Fig. 17. That figure does not appear to show a divergence as the technical cutoff is reduced. At first sight that may seem surprising, however two considerations should be kept in mind. Firstly, the configuration of Fig. 17 requires an initial-state gluon to originate from a $b \rightarrow gb$ splitting, which is responsible for only a small fraction of incoming gluons. Secondly, the impact of the IRC unsafety is to smear the rapidity distribution of the b -jet and a smearing of broad distribution tends to have a limited impact

Finally, note that the flavour- k_t algorithm does not suffer from the issue presented here thanks to the form of its beam distance: the initial-state emissions 1 and 2 would be declared as beam jets and so be removed from further consideration early in the clustering sequence.

3. IHC×IDS issue at α_s^3 for CMP

The subtlety from Sec. C 1 for the flavour- k_t and GHS algorithms has an interesting manifestation in the CMP algorithm. We consider again the scenario of Fig. 15, with the same set of variables and in a configuration where $p_{t4} \ll p_{t2}$. We will concentrate on the two distances that are smallest, which, neglecting $\mathcal{O}(1)$ factors, read

$$d_{23} \sim \frac{p_{t2}^2}{z_{23}^2 p_{t1}^4}, \quad d_{24} \sim \frac{p_{t2}^2}{p_{t1}^4} y_4^2. \quad (\text{C21})$$

As before, the probability for a 2+4 recombination must be finite for IRC safety. The 2+4 recombination will occur if

$$z_{23} \lesssim \frac{1}{y_4} = \frac{1}{\ell_{14} + \ln 2 z_{41}}. \quad (\text{C22})$$

We neglect the $\ln 2 z_{41}$ term in the denominator (and take the z_{41} integral to give a constant), integrate over all p_{t4} values, over $p_{t2} > p_{t4}$ and over the allowed z_{23} range (with the same constant splitting function approximation as in App. C 1). We then obtain the probability for a 2+4 clustering

$$N_{24} \sim \alpha_s^3 \int_0^\infty d\ell_{14} \int_0^{\ell_{14}} d\ell_{24} \int_0^{1/\ell_{14}} dz_{23}, \quad (\text{C23})$$

which is divergent. If we regulate the upper integration region of the ℓ_{14} integral with $\infty \rightarrow \ln \frac{1}{\epsilon}$, the probability scales as

$$N_{24} \sim \alpha_s^3 \ln \frac{1}{\epsilon}. \quad (\text{C24})$$

As with the other occurrences of this kind of issue, the replacement Eq. (11) solves the problem, as can be seen from the numerical IRC safety tests for this configuration shown in Fig. 19.

4. FHC² issue at α_s^2 for GHS

For the discussion here and in App. C 5, we assume a version of the GHS algorithm with an Ω_{ij}^2 style angular

on the integral of the broad distribution within some window (Ref. [10] used $|y_b| < 2.4$). As a result, it is conceivable that the expected squared logarithmic divergence in Fig. 1 (left) of Ref. [10] might be too small to clearly see in that figure.

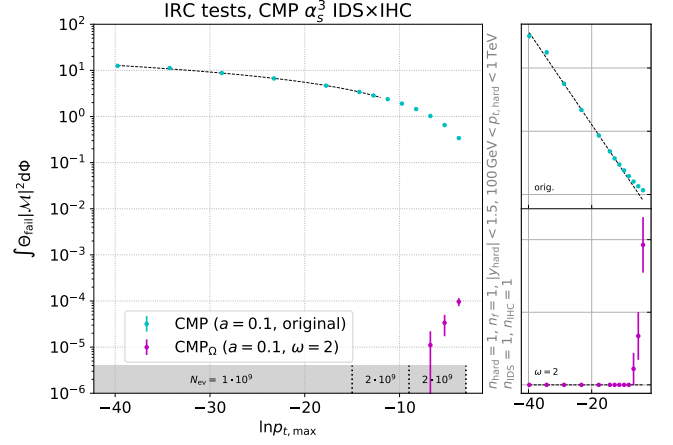


FIG. 19. Failure rate of the CMP algorithm for the configuration of Fig. 15, both for the original formulation and our modification, Eq. (11), showing a divergence for the former and none for the latter.

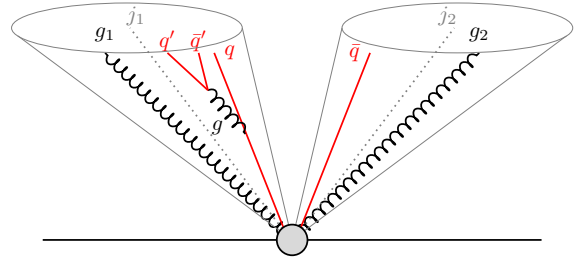


FIG. 20. Example $\mathcal{O}(\alpha_s^2)$ configuration that yields an issue for the GHS algorithm. There are four hard particles (that one can imagine recoiling against a hard gluon or electroweak system on the other side of the event), a collinear emission of a hard gluon g from one of the flavoured particles (the q), which then splits collinearly to a flavoured pair $q'\bar{q}'$.

distance in the dressing (flavour- k_t -like) phase, since we know from Sec. C 1 that this is required for the flavour- k_t algorithm, which is the basis of the algorithm's dressing step. To make this clear, in plots where this modification is used, we refer to the algorithm as GHS_Ω.

Let us consider a hard event as that in Fig. 20. The event has four particles, which we will call g_1 , q , \bar{q} and g_2 , starting from the left. We will work through the algorithm to see what happens if a hard, but collinear gluon g , is emitted from the q , and splits collinearly to $q'\bar{q}'$ (with $\Delta R_{q'\bar{q}'} \ll 1$ much smaller than any other scale in the problem).

Focusing on the hard event first (i.e. without the emission of the hard collinear gluon g), we assume that the anti- k_t algorithm clusters the four particles into two jets (j_1 and j_2), as indicated in the figure. We can further assume that $\Delta R_{g_1 q}, \Delta R_{g_2 \bar{q}} > R_{\text{cut}} \sim 0.1$, so that the hard gluons g_1 and g_2 are not accumulated into q and \bar{q} in that phase of the algorithm.

First we will consider the case $\alpha < 2$. For any angular structure of the event satisfying the above limits, we take

the momenta of g_1, g_2, q and \bar{q} such that the event without the $g \rightarrow q'\bar{q}'$ emission has the following properties

$$d_{qj_1} > d_{q\bar{q}} > d_{\bar{q}j_2}, \quad (\text{C25a})$$

$$p_{tq} < p_{t\bar{q}}. \quad (\text{C25b})$$

As a result, the first dressing step is for the \bar{q} flavour to be assigned to jet j_2 , followed by the q flavour being assigned to jet j_1 . Thus both j_1 and j_2 are flavoured. Note that for a full analysis, one should also take into account d_{iB} beam distances for all flavoured particles i . To help understand why we can ignore it, suppose that all the hard particles have rapidities close to zero, which results in $p_{tB}(0)$ in Eq. (C4) being approximately the scalar sum of all the particles' transverse momenta. That scale will tend to be a few times larger than the transverse momenta of any of the individual particles, which ensures that the distance of any cluster to its jet will be smaller than the d_{iB} , as will the $d_{q\bar{q}}$ if the two jets are not too far away in angle.

Next we consider the impact of the emission of the collinear hard gluon from q with $p_{tg} = zp_{tq}$, followed by its splitting into a collinear $q'\bar{q}'$ pair. Recall that we work with $\Delta R_{q'\bar{q}'} \ll R_{\text{cut}}$ so that it is the smallest angular distance in the event. The algorithm goes through the accumulation step, and will identify four flavour clusters: \hat{q}' , $\hat{\bar{q}}'$, and the original \hat{q} and $\hat{\bar{q}}$. The angular structure is otherwise unchanged, so we get no further flavour accumulation. To lighten the notation, below we will leave out the explicit “hats” for the flavour clusters, especially as the flavour clusters coincide with the original particles.

The final step is the flavour dressing: the q', \bar{q}' pair will annihilate first, as it should because the pair came from a common parent gluon. These flavour clusters (including their kinematics) are discarded from further consideration, and any distance involving them is removed from the list. The remaining distances (d') for the event with the $g \rightarrow q'\bar{q}'$ splitting are then given in terms of the hard-event's distances (d) as

$$d'_{qj_1} = (1-z)^{2-\alpha} d_{qj_1}, \quad (\text{C26a})$$

$$d'_{q\bar{q}} = (1-z)^{2-\alpha} d_{q\bar{q}}, \quad (\text{C26b})$$

$$d'_{\bar{q}j_2} = d_{\bar{q}j_2}, \quad (\text{C26c})$$

where the $(1-z)^{2-\alpha}$ factor arises because of the reduction in transverse momentum of the q after emission of the $g \rightarrow q'\bar{q}'$ (which carries a fraction z of its original q momentum). The potentially dangerous scenario is that where the ordering of distances, Eq. (C25a), is modified,

$$d'_{q\bar{q}} < \min(d'_{qj_1}, d'_{\bar{q}j_2}), \quad (\text{C27})$$

because then q and \bar{q} 's flavours will annihilate, leaving flavourless hard jets, associated with a squared logarithmic divergence from the two nested hard collinear divergences. There is a finite range of z in which this occurs,

$$1-z < \left(\frac{d_{\bar{q}j_2}}{d_{q\bar{q}}} \right)^{\frac{1}{2-\alpha}}, \quad (\text{C28})$$

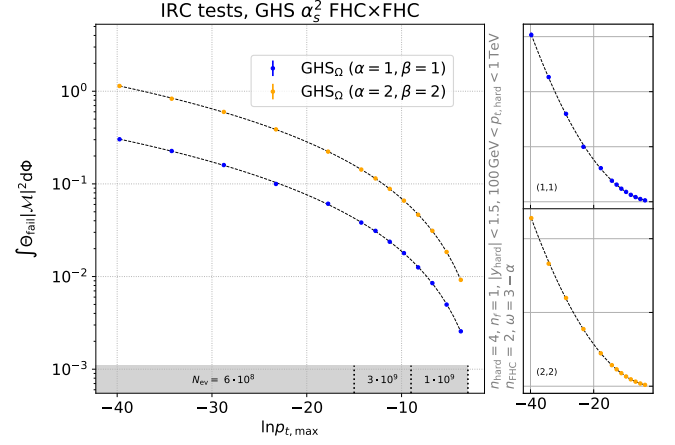


FIG. 21. Failure rate of the GHS algorithm for the FHCx FHC configuration of Fig. 20, illustrating the quadratic divergence, specifically for $\alpha = 1, \beta = 1$ and $\alpha = 2, \beta = 2$. Other parameters are $R_{\text{cut}} = 0.1$, $z_{\text{cut}} = 0.1$ and $p_{t,\text{cut}} = 100$ GeV. The jet radius R has been sampled in the range 0.3–1.57. The version of the GHS algorithm used is one where ΔR_{ij}^2 in the dressing stage has been replaced with Ω_{ij}^2 using $\omega = 3 - \alpha$ (the original ΔR_{ij}^2 similarly gives a squared logarithmic divergence).

thus confirming the presence of IRC unsafety from the configuration of Fig. 20 for $\alpha < 2$.

When $\alpha = 2$, we instead consider a hard event satisfying $p_{tq} > p_{t\bar{q}}$ rather than the inequality in Eq. (C25b), in which case we have

$$d'_{qj_1} = d_{qj_1}, \quad (\text{C29a})$$

$$d'_{q\bar{q}} = \max \left((1-z)^2, \frac{p_{t\bar{q}}^2}{p_{tq}^2} \right) d_{q\bar{q}}, \quad (\text{C29b})$$

$$d'_{\bar{q}j_2} = d_{\bar{q}j_2}. \quad (\text{C29c})$$

Again, there is the possibility of $d'_{q\bar{q}}$ becoming the smallest of the three distances, with the outcome that the q and \bar{q} flavours would annihilate, leaving flavourless hard jets, with a squared logarithmic divergence associated with the collinear splittings.

The set of distances in the argument above is perhaps somewhat complicated, with angular factors to consider, the beam distances and the extra subtleties of the $\alpha = 2$ case. Therefore, in Fig. 21 we show the outcome of our IRC safety tests, illustrating that the divergence is indeed present for the two combinations $\alpha = 1, \beta = 1$ and $\alpha = 2, \beta = 2$. We leave to future work the possibility of identifying a concrete modification of the algorithm that solves this problem, nevertheless we anticipate that one line of investigation could be to allow accumulation of kinematics within a jet during the dressing stage.

A final comment is that this configuration can appear at NNLO for a process such as fully hadronic $t\bar{t}$ production, however only if one asks for two massive b -tagged jets. It also appears at N⁴LO for a process such as $Zb\bar{b}$ production.

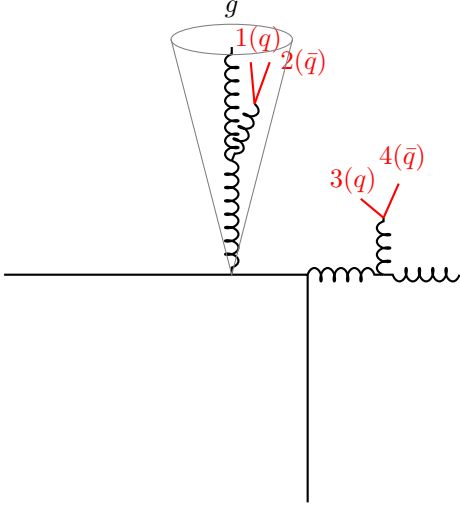


FIG. 22. An FDSxIDS kinematic configuration that causes problems for GHS algorithms for $\alpha\beta \geq 2$.

5. IDSxIDS issue at α_s^4 for GHS

The GHS algorithm exhibits an interesting interplay between initial-state and final-state double-soft emissions at order α_s^4 if $\alpha\beta \geq 2$. The configuration that we consider here is that represented in Fig. 22, involving a hard Born event with one or more unflavoured jets. That event is then supplemented with a double-soft pair (1,2) that is collinear to an (originally) unflavoured jet and an additional large-angle double-soft pair (3,4) outside the jet.

We are specifically interested in the situation where

$$\theta_{1g} \lesssim \{\theta_{2g}, \theta_{12}\} \ll 1, \quad (\text{C30a})$$

$$p_{t1} \sim p_{t2} \ll p_{tg}, \quad (\text{C30b})$$

$$p_{t3} \sim p_{t4} \ll p_{tg}, \quad (\text{C30c})$$

$$\theta_{23} \sim \theta_{34} \sim 1. \quad (\text{C30d})$$

During the accumulation step, there is a possibility that 1 clusters with g , giving a hard $\widehat{g1}$ flavour cluster, leaving an unclustered, much softer $\widehat{2}$ flavour cluster. If during the subsequent dressing phase, $\widehat{2}$ goes on to annihilate with $\widehat{3}$ rather than with $\widehat{g1}$, then the resulting hard jet will be flavoured.

The SoftDrop condition for 1 to cluster with g is given by

$$\frac{p_{t1}}{p_{tg}} > \theta_{1g}^\beta, \quad (\text{C31})$$

where throughout our discussion here we neglect factors of order 1 (e.g. R_{cut} and z_{cut}). There is no further accumulation since all particles are now flavoured and the flavoured clusters will be $\widehat{g1}$, $\widehat{2}$, $\widehat{3}$ and $\widehat{4}$. The angle between the $\widehat{g1}$ and the jet direction will be given by

$$\theta_{j\widehat{g1}} \sim \frac{p_{t2}}{p_{tg}} \theta_{2g}. \quad (\text{C32})$$

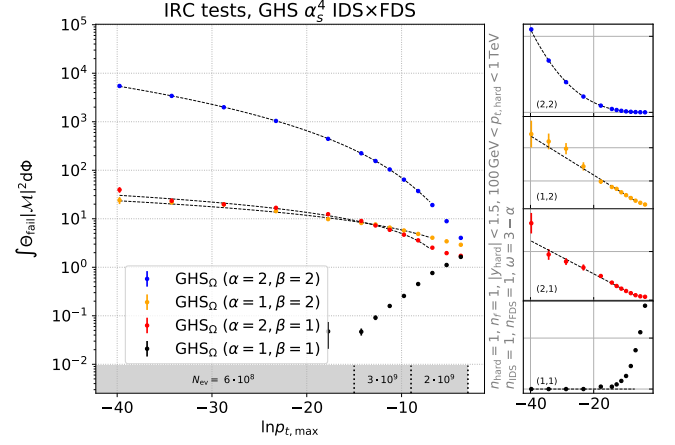


FIG. 23. Failure rate of the GHS algorithm for the α_s^4 FDSxIDS configuration of Fig. 22, illustrating the cubic divergence for parameter choices involving $\alpha\beta > 2$, the linear divergence for $\alpha\beta = 2$ and convergence for $\alpha\beta < 2$. In its dressing stage, the GHS implementation for these runs uses an Ω_{ij}^2 angular distance instead of ΔR_{ij}^2 , where $\omega = 3 - \alpha$. Other parameters are $R_{\text{cut}} = 0.1$, $z_{\text{cut}} = 0.1$ and $p_{t,\text{cut}} = 100$ GeV.

Without loss of generality we can consider the case where $d_{23} < d_{24}$, and then the distances to take into account during the dressing phase are

$$d_{j\widehat{g1}} \sim p_{t2}^2 \theta_{2g}^2, \quad (\text{C33a})$$

$$d_{g1\widehat{2}} \sim d_{j\widehat{2}} \sim p_{tg}^2 \left(\frac{p_{t2}}{p_{tg}} \right)^{2-\alpha} \theta_{2g}^2, \quad (\text{C33b})$$

$$d_{2\widehat{3}} \sim \max(p_{t2}, p_{t3})^\alpha \min(p_{t2}, p_{t3})^{2-\alpha}, \quad (\text{C33c})$$

$$d_{3\widehat{4}} \sim p_{t3}^2, \quad (\text{C33d})$$

where, again we have ignored factors of order 1, e.g. from angular distances. The hard jet will acquire a flavour if the SoftDrop condition of Eq. (C31) is satisfied and if additionally $\widehat{2}$ fails to annihilate the flavour of the $\widehat{g1}$ cluster. This will occur if $d_{23} < d_{34}$ and $d_{23} < d_{j\widehat{2}} \simeq d_{g1\widehat{2}}$.¹⁹ In determining whether these conditions are satisfied, it is helpful to introduce shorthands

$$\ell_i = \ln \frac{p_{tg}}{p_{ti}}, \quad (\text{C34a})$$

$$\ell_\theta = \ln \frac{1}{\theta_{2g}}, \quad (\text{C34b})$$

and to observe that in the SoftDrop condition Eq. (C31), we can replace $1 \rightarrow 2$, since this only affects $\mathcal{O}(1)$ terms.

¹⁹ Note that the $d_{23} < d_{34}$ condition implies that p_{t2} cannot be substantially larger than p_{t3} , which leads to $d_{j\widehat{g1}}$ being the smallest of all the distances. Consequently, the first step of the dressing is that the flavour of $\widehat{g1}$ is assigned to the jet and the $\widehat{g1}$ cluster is removed from consideration.

Our conditions then become (to within $\mathcal{O}(1)$ offsets)

$$\text{SD : } \ell_2 < \beta \ell_\theta, \quad (\text{C35a})$$

$$d_{34} > d_{23} : \ell_2 > \ell_3, \quad (\text{C35b})$$

$$d_{g2} > d_{23} : (2 - \alpha)\ell_2 + 2\ell_\theta < \alpha\ell_3 + (2 - \alpha)\ell_2, \quad (\text{C35c})$$

where the last line already underwent some simplification (using the second line), and can then be further simplified to read

$$2\ell_\theta < \alpha\ell_3. \quad (\text{C36})$$

Assembling all inequalities, we obtain

$$2\ell_\theta < \alpha\ell_3 < \alpha\ell_2 < \alpha\beta\ell_\theta. \quad (\text{C37})$$

We immediately see that if $\alpha\beta < 2$, there is no available logarithmic integration region, and so no IRC divergence from this configuration. Conversely, if $\alpha\beta > 2$, we expect to see a cubic logarithmic divergence from integrals over ℓ_θ , ℓ_3 and ℓ_2 . For $\alpha\beta = 2$, the $\mathcal{O}(1)$ factors become critical and it is easiest to carry out a numerical study, but it is reasonable to expect a divergence with a single logarithm.

The results of the numerical study are shown in Fig. 23 for four combinations of α and β . They confirm our expectations and suggest that if one wishes to employ a GHS-style algorithm, one should use it with $\alpha\beta < 2$. Nevertheless, one would still need to find a solution to the separate issue identified in App. C 4 (which cannot be resolved just through parameter choices), and then verify that the resulting algorithm passes a full set of IRC safety tests.

Appendix D: Summary plots for IRC-safe algorithms

In this appendix, we present summary plots from our IRC safety tests for the three approaches that have passed all those tests: IFN, CMP_Ω and flavour- $k_{t,\Omega}$. In Figs. 24 and 25, we show the results from the IRC-safety tests for the anti- k_t and C/A algorithms with IFN, i.e. each of the algorithms labelled as safe in Table I. Figs. 26 and 27 show corresponding results for our adaptations of the flavour- k_t and CMP algorithms, supporting the conclusion that they too are IRC safe.

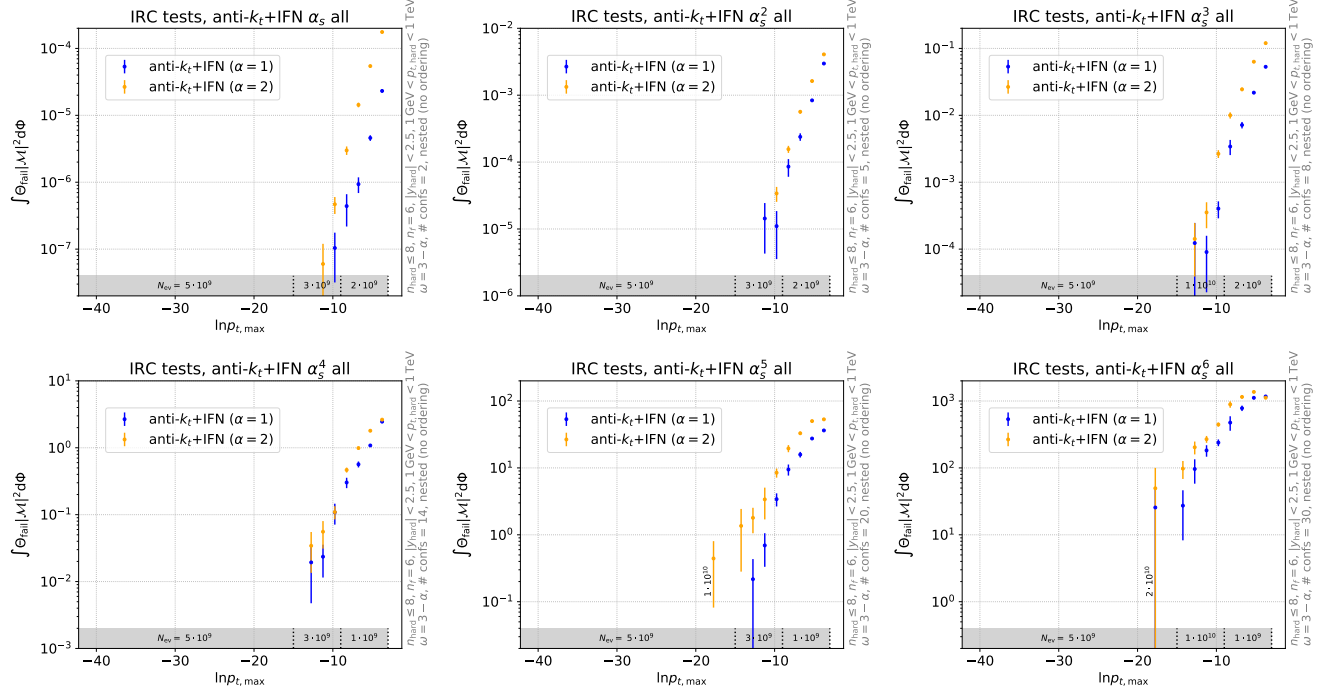


FIG. 24. Summary of IRC safety test results at orders α_s to α_s^6 for the anti- k_t algorithm with IFN.

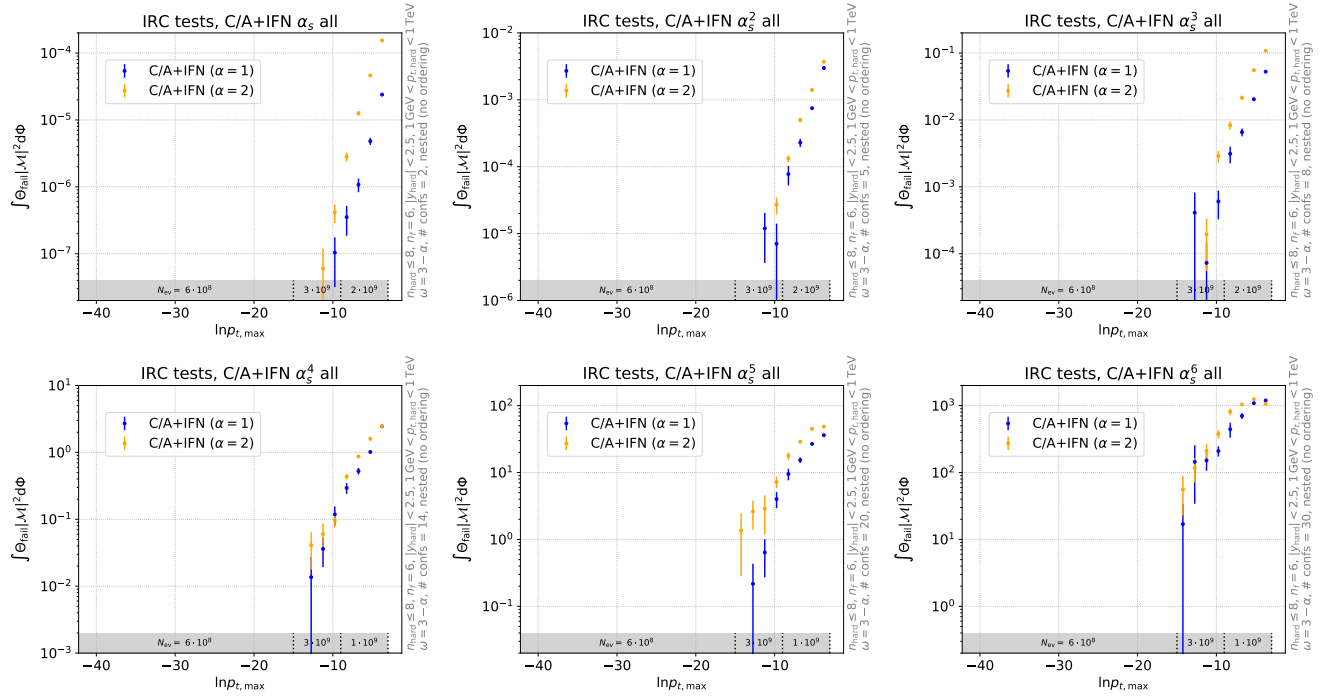
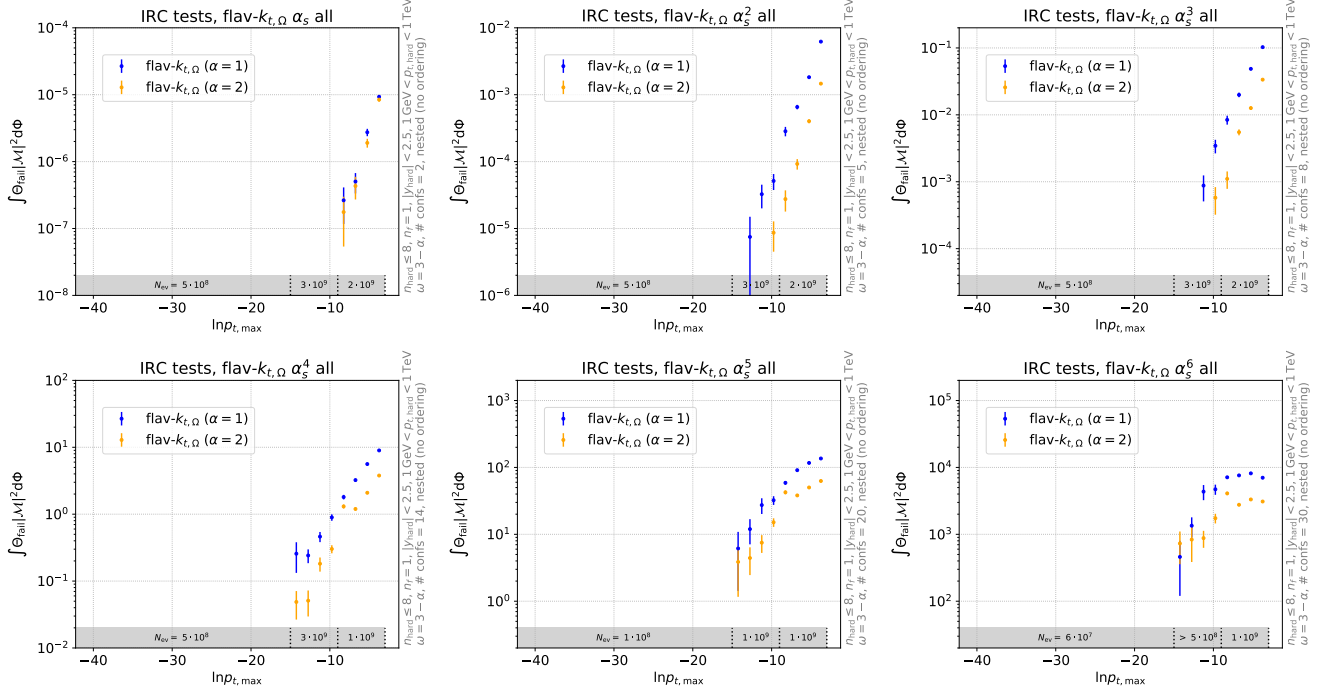
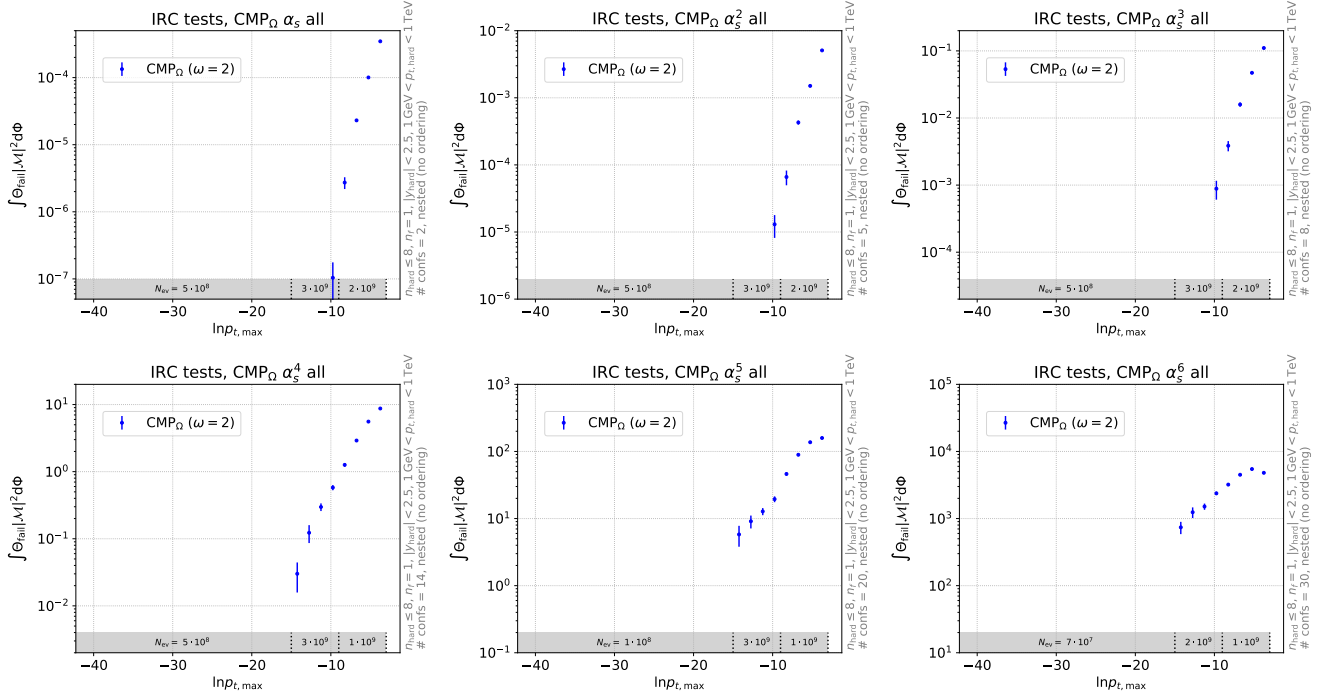


FIG. 25. Same as Fig. 24, for the C/A algorithm with IFN.

FIG. 26. Same as Fig. 24, for the flavour- $k_{t,\Omega}$ algorithm.FIG. 27. Same as Fig. 24, for the CMP_{Ω} algorithm.

-
- [1] A. Banfi, G. P. Salam, and G. Zanderighi, *Infrared safe definition of jet flavor*, *Eur. Phys. J. C* **47** (2006) 113–124, [[hep-ph/0601139](#)].
- [2] A. Banfi, G. P. Salam, and G. Zanderighi, *Accurate QCD predictions for heavy-quark jets at the Tevatron and LHC*, *JHEP* **07** (2007) 026, [[arXiv:0704.2999](#)].
- [3] S. Catani, Y. L. Dokshitzer, M. Olsson, G. Turnock, and B. R. Webber, *New clustering algorithm for multi-jet cross-sections in e^+e^- annihilation*, *Phys. Lett. B* **269** (1991) 432–438.
- [4] S. Catani, Y. L. Dokshitzer, M. H. Seymour, and B. R. Webber, *Longitudinally invariant K_t clustering algorithms for hadron hadron collisions*, *Nucl. Phys. B* **406** (1993) 187–224.
- [5] S. D. Ellis and D. E. Soper, *Successive combination jet algorithm for hadron collisions*, *Phys. Rev. D* **48** (1993) 3160–3166, [[hep-ph/9305266](#)].
- [6] M. Cacciari, G. P. Salam, and G. Soyez, *The anti- k_t jet clustering algorithm*, *JHEP* **04** (2008) 063, [[arXiv:0802.1189](#)].
- [7] R. Gauld, A. Gehrmann-De Ridder, E. W. N. Glover, A. Huss, and I. Majer, *Predictions for Z-Boson Production in Association with a b-Jet at $\mathcal{O}(\alpha_s^3)$* , *Phys. Rev. Lett.* **125** (2020), no. 22 222002, [[arXiv:2005.03016](#)].
- [8] S. Caletti, A. J. Larkoski, S. Marzani, and D. Reichelt, *Practical jet flavour through NNLO*, *Eur. Phys. J. C* **82** (2022), no. 7 632, [[arXiv:2205.01109](#)].
- [9] S. Caletti, A. J. Larkoski, S. Marzani, and D. Reichelt, *A fragmentation approach to jet flavor*, *JHEP* **10** (2022) 158, [[arXiv:2205.01117](#)].
- [10] M. Czakon, A. Mitov, and R. Poncelet, *Infrared-safe flavoured anti- k_T jets*, *JHEP* **04** (2023) 138, [[arXiv:2205.11879](#)].
- [11] R. Gauld, A. Huss, and G. Stagnitto, *Flavor Identification of Reconstructed Hadronic Jets*, *Phys. Rev. Lett.* **130** (2023), no. 16 161901, [[arXiv:2208.11138](#)].
- [12] S. Weinzierl, *The Forward-backward asymmetry at NNLO revisited*, *Phys. Lett. B* **644** (2007) 331–335, [[hep-ph/0609021](#)].
- [13] Z. Trócsányi, G. Somogyi, and F. Tramontano, *Fully Differential Decay Rate of a Standard Model Higgs Boson into Two b-jets at NNLO*, *Acta Phys. Polon. B* **46** (2015), no. 11 2097.
- [14] G. Ferrera, G. Somogyi, and F. Tramontano, *Associated production of a Higgs boson decaying into bottom quarks at the LHC in full NNLO QCD*, *Phys. Lett. B* **780** (2018) 346–351, [[arXiv:1705.10304](#)].
- [15] F. Caola, G. Luisoni, K. Melnikov, and R. Rötsch, *NNLO QCD corrections to associated WH production and $H \rightarrow b\bar{b}$ decay*, *Phys. Rev. D* **97** (2018), no. 7 074022, [[arXiv:1712.06954](#)].
- [16] R. Gauld, A. Gehrmann-De Ridder, E. W. N. Glover, A. Huss, and I. Majer, *Associated production of a Higgs boson decaying into bottom quarks and a weak vector boson decaying leptonically at NNLO in QCD*, *JHEP* **10** (2019) 002, [[arXiv:1907.05836](#)].
- [17] M. Czakon, A. Mitov, M. Pellen, and R. Poncelet, *NNLO QCD predictions for $W+c$ -jet production at the LHC*, *JHEP* **06** (2021) 100, [[arXiv:2011.01011](#)].
- [18] H. B. Hartanto, R. Poncelet, A. Popescu, and S. Zoia, *Next-to-next-to-leading order QCD corrections to $Wb\bar{b}$ production at the LHC*, *Phys. Rev. D* **106** (2022), no. 7 074016, [[arXiv:2205.01687](#)].
- [19] H. B. Hartanto, R. Poncelet, A. Popescu, and S. Zoia, *Flavour anti- k_T algorithm applied to $Wb\bar{b}$ production at the LHC*, [arXiv:2209.03280](#).
- [20] M. Czakon, A. Mitov, M. Pellen, and R. Poncelet, *A detailed investigation of $W+c$ -jet at the LHC*, *JHEP* **02** (2023) 241, [[arXiv:2212.00467](#)].
- [21] R. Gauld, A. Gehrmann-De Ridder, E. W. N. Glover, A. Huss, A. R. Garcia, and G. Stagnitto, *NNLO QCD predictions for Z-boson production in association with a charm jet within the LHCb fiducial region*, *Eur. Phys. J. C* **83** (2023), no. 4 336, [[arXiv:2302.12844](#)].
- [22] Y. L. Dokshitzer, G. D. Leder, S. Moretti, and B. R. Webber, *Better jet clustering algorithms*, *JHEP* **08** (1997) 001, [[hep-ph/9707323](#)].
- [23] M. Wobisch and T. Wengler, *Hadronization corrections to jet cross-sections in deep inelastic scattering*, in *Workshop on Monte Carlo Generators for HERA Physics (Plenary Starting Meeting)*, pp. 270–279, 4, 1998. [hep-ph/9907280](#).
- [24] S. Hoeche, F. Krauss, S. Schumann, and F. Siegert, *QCD matrix elements and truncated showers*, *JHEP* **05** (2009) 053, [[arXiv:0903.1219](#)].
- [25] A. Karlberg, G. P. Salam, L. Scyboz, and R. Verheyen, *Spin correlations in final-state parton showers and jet observables*, *Eur. Phys. J. C* **81** (2021), no. 8 681, [[arXiv:2103.16526](#)].
- [26] M. van Beekveld, S. Ferrario Ravasio, K. Hamilton, G. P. Salam, A. Soto-Ontoso, G. Soyez, and R. Verheyen, *PanScales showers for hadron collisions: all-order validation*, *JHEP* **11** (2022) 020, [[arXiv:2207.09467](#)].
- [27] G. P. Salam and G. Soyez, *A Practical Seedless Infrared-Safe Cone jet algorithm*, *JHEP* **05** (2007) 086, [[arXiv:0704.0292](#)].
- [28] J. Gallicchio and Y.-T. Chien, *Quit Using Pseudorapidity, Transverse Energy, and Massless Constituents*, [arXiv:1802.05356](#).
- [29] A. Buckley and C. Pollard, *QCD-aware partonic jet clustering for truth-jet flavour labelling*, *Eur. Phys. J. C* **76** (2016), no. 2 71, [[arXiv:1507.00508](#)].
- [30] JADE Collaboration, W. Bartel et al., *Experimental Studies on Multi-Jet Production in e^+e^- Annihilation at PETRA Energies*, *Z. Phys. C* **33** (1986) 23.
- [31] JADE Collaboration, S. Bethke et al., *Experimental Investigation of the Energy Dependence of the Strong Coupling Strength*, *Phys. Lett. B* **213** (1988) 235–241.
- [32] A. Behring, W. Bizoń, F. Caola, K. Melnikov, and R. Rötsch, *Bottom quark mass effects in associated WH production with the $H \rightarrow b\bar{b}$ decay through NNLO QCD*, *Phys. Rev. D* **101** (2020), no. 11 114012, [[arXiv:2003.08321](#)].
- [33] A. J. Larkoski, S. Marzani, G. Soyez, and J. Thaler, *Soft Drop*, *JHEP* **05** (2014) 146, [[arXiv:1402.2657](#)].
- [34] B. Andersson, G. Gustafson, L. Lonnblad, and U. Pettersson, *Coherence Effects in Deep Inelastic Scattering*, *Z. Phys. C* **43** (1989) 625.

- [35] M. Cacciari, G. P. Salam, and G. Soyez, *FastJet User Manual*, *Eur. Phys. J. C* **72** (2012) 1896, [[arXiv:1111.6097](#)].
- [36] Y. Hida, X. S. Li, and D. H. Bailey, *Quad-double arithmetic: Algorithms, implementation, and application*, in *15th IEEE Symposium on Computer Arithmetic*, pp. 155–162, 2000.
- [37] M. Dasgupta, F. A. Dreyer, K. Hamilton, P. F. Monni, G. P. Salam, and G. Soyez, *Parton showers beyond leading logarithmic accuracy*, *Phys. Rev. Lett.* **125** (2020), no. 5 052002, [[arXiv:2002.11114](#)].
- [38] K. Hamilton, R. Medves, G. P. Salam, L. Scyboz, and G. Soyez, *Colour and logarithmic accuracy in final-state parton showers*, *JHEP* **03** (2021), no. 041 041, [[arXiv:2011.10054](#)].
- [39] CMS Collaboration, A. M. Sirunyan et al., *Evidence for the Higgs boson decay to a bottom quark-antiquark pair*, *Phys. Lett. B* **780** (2018) 501–532, [[arXiv:1709.07497](#)].
- [40] ATLAS Collaboration, G. Aad et al., *Measurements of WH and ZH production in the $H \rightarrow b\bar{b}$ decay channel in pp collisions at 13 TeV with the ATLAS detector*, *Eur. Phys. J. C* **81** (2021), no. 2 178, [[arXiv:2007.02873](#)].
- [41] ATLAS Collaboration, G. Aad et al., *Measurement of the associated production of a Higgs boson decaying into b -quarks with a vector boson at high transverse momentum in pp collisions at $\sqrt{s} = 13$ TeV with the ATLAS detector*, *Phys. Lett. B* **816** (2021) 136204, [[arXiv:2008.02508](#)].
- [42] CMS Collaboration, A. M. Sirunyan et al., *Inclusive search for highly boosted Higgs bosons decaying to bottom quark-antiquark pairs in proton-proton collisions at $\sqrt{s} = 13$ TeV*, *JHEP* **12** (2020) 085, [[arXiv:2006.13251](#)].
- [43] J. M. Butterworth, A. R. Davison, M. Rubin, and G. P. Salam, *Jet substructure as a new Higgs search channel at the LHC*, *Phys. Rev. Lett.* **100** (2008) 242001, [[arXiv:0802.2470](#)].
- [44] S. Marzani, G. Soyez, and M. Spannowsky, *Looking inside jets: an introduction to jet substructure and boosted-object phenomenology*, vol. 958. Springer, 2019.
- [45] T. Sjöstrand, S. Ask, J. R. Christiansen, R. Corke, N. Desai, P. Ilten, S. Mrenna, S. Prestel, C. O. Rasmussen, and P. Z. Skands, *An introduction to PYTHIA 8.2*, *Comput. Phys. Commun.* **191** (2015) 159–177, [[arXiv:1410.3012](#)].
- [46] C. Bierlich et al., *A comprehensive guide to the physics and usage of PYTHIA 8.3*, [arXiv:2203.11601](#).
- [47] R. Corke and T. Sjostrand, *Interleaved Parton Showers and Tuning Prospects*, *JHEP* **03** (2011) 032, [[arXiv:1011.1759](#)].
- [48] P. Skands, S. Carrazza, and J. Rojo, *Tuning PYTHIA 8.1: the Monash 2013 Tune*, *Eur. Phys. J. C* **74** (2014), no. 8 3024, [[arXiv:1404.5630](#)].
- [49] P. Gras, S. Höche, D. Kar, A. Larkoski, L. Lönnblad, S. Plätzer, A. Siódmok, P. Skands, G. Soyez, and J. Thaler, *Systematics of quark/gluon tagging*, *JHEP* **07** (2017) 091, [[arXiv:1704.03878](#)].
- [50] M. Dasgupta, F. Dreyer, G. P. Salam, and G. Soyez, *Small-radius jets to all orders in QCD*, *JHEP* **04** (2015) 039, [[arXiv:1411.5182](#)].
- [51] S. Catani and M. H. Seymour, *A General algorithm for calculating jet cross-sections in NLO QCD*, *Nucl. Phys. B* **485** (1997) 291–419, [[hep-ph/9605323](#)]. [Erratum: *Nucl.Phys.B* 510, 503–504 (1998)].
- [52] M. van Beekveld, W. Beenakker, E. Laenen, and C. D. White, *Next-to-leading power threshold effects for inclusive and exclusive processes with final state jets*, *JHEP* **03** (2020) 106, [[arXiv:1905.08741](#)].